4-2002

Design and Construction of a Radio Frequency Plasma Device

Matthew Highland '02
Illinois Wesleyan University

Design and Construction of a Radio Frequency Plasma Device

by

Matthew J. Highland

Submitted to the Department of Physics
in partial fulfillment of the requirements for Research Honors

at

Illinois Wesleyan University

April 2002

Author: Matt Highland
Department of Physics
4/30/02

Certified by:
Jeremiah Williams
Reader

Certified by: W J Detweiler
Dr. Lew Detweiler
Reader

Certified by: Narendra Jaggi 4-30-02
Dr. Narendra K. Jaggi
Reader

Certified by:
Dr. Timothy Rettich
Reader

Certified by:
Dr. Gaberiel C. Spalding
Reader

DESIGN AND CONSTRUCTION OF A RADIO FREQUENCY PLASMA DEVICE

Matt Highland, Jeremiah Williams*

Department of Physics, Illinois Wesleyan University

We have constructed a radio frequency plasma device to study a wide range of phenomena including, power coupling between the plasma and the antenna and wave propagation. Our system includes a high vacuum chamber with mechanical and diffusion pumps, a radio frequency source magnetic field coils and a matching network.

Acknowledgments

I would to thank the entire physics department for their time and insight, Prof. Stranberg for his practical advice, my thesis review board for there helpful comments. And I would especially like to thank my girlfriend Ariane for her unending support, insight, and mechanical expertise.

Contents

Table of Figures

Chapter 1

Introduction

When a student encounters the concept of matter they are often told that the world around us is composed of matter, which exists in one of four phases. We then proceed to study the behavior of solids, liquids, and gases in great detail. A good student will likely notice that left out of our detailed investigation of matter is the fourth, and often forgotten, state: plasma.

Plasma is a state of matter in which the rate of particle ionization greatly exceeds the rate of recombination. A more formal definition is given by Chen, "A plasma is a quasi-neutral gas of charged and neutral particles which exhibits collective behavior."[1] "Quasi-neutral" means that the number of positively charged ions and electrons are of the same order so that the plasma does not contain large potentials. This definition is a bit outdated though; recent experiments have been done with plasmas made completely of ion, or of electrons [4]. The "electron gas" in a metal also behaves as a plasma. The distinction is that even though these non-neutral systems behave much like plasmas, they technically are not. Requiring that a plasmas "exhibit collective behavior" alludes to the fact that the local behavior of a plasma is governed not by local interactions, *i.e.* collisions as in a normal gas, but rather by long range electromagnetic forces.

Plasmas occur throughout the universe at a variety of temperatures and densities. Despite this fact, plasmas are not very common on earth. We can examine the ratio of the density of ionized particles, n_i ,to the density of neutral atoms, n_n, given by the Saha equation [1]:

$$\frac{n_i}{n_n} \approx 2.4\times10^{21}\frac{T^{3/2}}{n_i}e^{-U_i/kT} \tag{1}$$

where T is temperature, k is Boltzman's constant, and U_i is the ionization energy. At normal atmospheric conditions the ratio for nitrogen is 10^{-122}. The ambient conditions on earth are far from those needed to create plasma, thus explaining their absence. Figure 1 depicts a variety of plasmas as a function of their temperature and density.

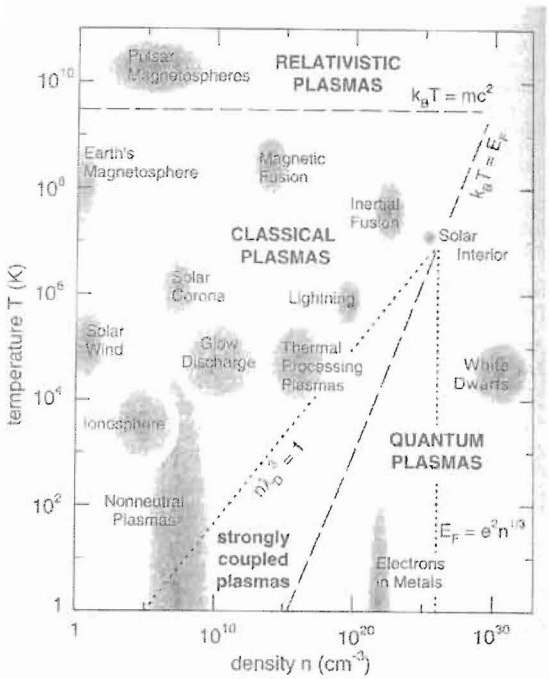

Figure 1: Occurrences of plasmas at different temperatures and densities|4|

In recent, years research in plasma physics has had a strong emphasis placed on fusion by organizations like the Department of Energy. Though beneficial to many of the technological aspects of plasma research, this has resulted in less emphasis being placed on the understanding of the underlying physics. In 1992, the National Research Council began a study to find ways to close the gap between basic plasma research and plasma technology [4]. The primary suggestion of the NRC was to return plasma research to the small university setting, helping to close the gap between the theoretical development of plasma physics and the ever growing demand for plasma application.

Beyond fusion applications, plasmas have found many additional applications in industry. Semiconductor manufacturers use plasmas to etch the silicon wafers needed for microchips. In the past manufactures have acid etched silicon wafers. Problems arise with this method when acids under cut wafers at the edges. Highly unidirectional ions produced by plasmas are used to etch wafers by bombarding the silicon surface [3]. A better theory of plasma production would allow semi-conductor manufactures to control certain plasma parameters, which would in turn improve the quality of semiconductors. Plasmas also hold great promise in the area of space propulsion [4]. Charged particles can be accelerated through a potential difference and thrust out

of a system. This thrust can then be used for less expensive and efficient propulsion. Application of this concept hinges on better understanding of power coupling between helicon sources and plasmas, as well as creating plasmas without electrodes. Current concerns about the emission of greenhouse gases, has led to the use of plasmas for pollution reduction [4]. Placement of low temperature plasmas in industrial smoke stacks can reduce the release of SO_2 and NO_x.

All of these applications would benefit from a deeper understanding of plasma physics. Due to the highly nonlinear nature of plasmas, analytic work is limited to the linear regime. This leads to experimental and numerical studies as key mechanism to understanding and developing models of the underlying physics. To study plasmas in the laboratory, there are many mechanisms to create a plasma, including helicon waves. My thesis will discuss plasma production with helicon sources. Chapter 2 will discuss the history and development of the helicon source. Chapter 3 presents a theoretical treatment of helicon waves. Chapter 4 will discuss the I.W.U. plasma device. Chapter 5 will discuss the helicon source. Chapter 6 is on the plasma diagnostics, and chapter 7 will discuss future work.

Chapter 2

Helicon source

2.1 Why a helicon source?

The creation of a plasma in the laboratory setting can be achieved by a number of mechanisms. Large DC biases applied to a cathode and an anode can create electric fields strong enough to ionize gas between the plates [4]. High power lasers can be used to focus energy into a small volume, creating plasma [4]. One efficient mechanism for creating a laboratory plasma is through the use of helicon waves [7].

The helicon source is able to produce high-density plasmas at very low pressures, for modest energy expenditures. Often densities of $10^{12}cm^{-3}$ can be achieved with powers of 400W and background pressures of a few milli-Torr [6]. This makes the helicon source attractive for a number of applications. Helicon sources are also of interest because they are not fully understood [8]. One theory explains the efficiency by Landau damping in which highly energetic electrons are caught in helicon waves [1]. However, work by Chen has shown that not enough of these high energy electrons are present in helicon plasmas to account for their ionization efficiency [7]. Further research on power coupling and plasma modes in helicon sources are vital to constructing a theory to explain their high efficiency.

2.2 History of Helicon source

Helicon waves were first observed in Austria in 1886 on telephone lines at the Sonnblick High Altitude Observatory [11]. However, well documented accounts were not seen until the early 1900's. During WWI, Americans listening for enemy transmissions on shortwave radio reported hearing whistling tones, which would start as high pitches and descend. These tones were due to waves, known as whistler waves. Lightning would emit waves at many frequencies. It was later shown that lightning emitted right-handed polarized waves, which would then propagate parallel to the earth's magnetic field, through the ionosphere. The waves emitted at higher frequencies would reach the listeners before lower frequency waves, due to the dispersive nature of the ionosphere, creating the observed whistling tones.

When Aigrain[13] theorized that these waves could be observed in a solid state system, he renamed them as helicon waves because the polarized E-field traces a helix along magnetic field lines. This gave rise to the distinction that these right-handed polarized waves are called whistler waves when propagating in an "unbounded" medium and helicon waves when propagating in a bounded medium. The first laboratory experiments with helicon waves were done by Gallet on the ZETA torus fusion machine in Harwell, England [14]. These and other experiments hoped to use helicon waves as a plasma diagnostic. Boswell was first to use helicon waves as a plasma source [15]. Boswell used a double loop antenna with a 600W power source to produce plasma number densities up to 10^{12} cm^{-3}. Plasma became of interest to the electronics industry when Boswell and Henry suggested that they could be used for precision etching of semi-conductors [16]. This, in turn, lead to the many applications mentioned in chapter 1.

Chapter 3

A Theoretical Treatment of waves in plasmas

To understand the behavior of a wave, it is important to know it's dispersion relation, $\omega(k)$. The dispersion relation tells us the speed of the wave and how it responds to changes in the medium of propagation.

The speed of a wave in a plasma is affected by parameters such as the applied magnetic field, number density, and the charge of species in the medium. The effect that these parameters have on the wave can be found in the dispersion relation, making it essential to fully understanding of helicon plasma production. In the following sections I derive the dispersion relation for an unbounded helicon wave in cold magnetized plasma [1]. Taking the plasma to be unbounded implies there are no boundary conditions. We will then derive the same dispersion relation for a bound plasma [2], to account for boundary conditions that exist in the laboratory.

3.1 Derivation of dispersion relation of a Wave traveling in a Un-bound cold uniform plasma

Consider cold plasma in a region of uniform magnetic field pointing in the z direction. Since plasmas consist of charged particles that will rearrange in response to an applied field, plasmas behave as a dielectric. This rearrangement acts to screen the affects of applied potentials. Screening can be interpreted as polarization, similar to that seen in dielectrics.

As a plasma responds to an applied field the displacement current **j** is due to movement of charged species within the plasma. Therefore we can write:

$$\vec{j} = \sum_{s} n_s q_s \vec{v}_s \tag{1}$$

where n is number density, q is charge, and v is particle velocity. The sum is taken over all particle species, s, in the plasma. If we regard the plasma as a dielectric, j constitutes a

displacement current in the plasma. In the presence of oscillating electric fields the displacement field D is:

$$\vec{D} = \varepsilon_0 \vec{E} + \frac{i}{\omega}\vec{j} \tag{2}$$

Since current density, j, represents a displacement current, as such, it is proportional to the electric field:

$$\vec{j} = \vec{\vec{\sigma}} \cdot \vec{E} \tag{3}$$

where σ is the conductivity tensor. The displacement field then becomes:

$$\vec{D} = \varepsilon_0 \left(\vec{\vec{I}} + \frac{i}{\varepsilon_0 \omega}\vec{\vec{\sigma}} \right) \cdot \vec{E} \tag{4}$$

Above $\boldsymbol{I}$ is the unit tensor. By inspection, we can now define the dielectric tensor:

$$\vec{\vec{\varepsilon}} = \varepsilon_0 \left(\vec{\vec{I}} + \frac{i\vec{\vec{\sigma}}}{\varepsilon_0 \omega} \right) \tag{5}$$

To write the dielectric tensor in terms other that conductance, we must examine the motion of particles in the plasma.

In the cold plasmas, we may neglect pressures and collisions; reducing the fluid equations of motion to the Lorentz force law:

$$m_s \frac{d\vec{v}_s}{dt} = q_s \left(\vec{E} + \vec{v}_s \times B_0 \right) \tag{6}$$

where m_s is the mass of a specific particle and B_0 is the static background magnetic field. This equation can be separated into its components. From this, we can determine the velocity of a

particle in each direction, in terms of the electric fields. As we do, it is useful to define the cyclotron and plasma frequencies:

$$\omega_{cs} \equiv \left| \frac{q_s B_0}{m_s} \right| \tag{7}$$

$$\omega_{ps} \equiv \frac{n q_s^2}{\varepsilon_0 m_s} \tag{8}$$

This allows us to more compactly write the velocity components as:

$$v_{xs} = \frac{i q_s}{m_s \omega} \frac{\left[E_x \pm i(\omega_{cs}/\omega) E_y \right]}{1 - (\omega_{cs}/\omega)^2} \tag{9}$$

$$v_{ys} = \frac{i q_s}{m_s \omega} \frac{\left[E_y \mp i(\omega_{cs}/\omega) E_x \right]}{1 - (\omega_{cs}/\omega)^2} \tag{10}$$

$$v_{zs} = \frac{i q_s}{m_s \omega} \tag{11}$$

Equation (3) defines $\boldsymbol{j}$ in terms of $\boldsymbol{v}$. Algebra yields

$$\frac{i}{\varepsilon_0 \omega} j_x = -\frac{1}{2} \sum_s \frac{\omega_{ps}^2}{\omega^2} \left[\left(\frac{\omega}{\omega \mp \omega_{cs}} + \frac{\omega}{\omega \pm \omega_{cs}} \right) E_x + \left(\frac{\omega}{\omega \mp \omega_{cs}} - \frac{\omega}{\omega \pm \omega_{cs}} \right) i E_y \right] \tag{12}$$

$$\frac{i}{\varepsilon_0 \omega} j_y = -\frac{1}{2} \sum_s \frac{\omega_{ps}^2}{\omega^2} \left[\left(\frac{\omega}{\omega \pm \omega_{cs}} + \frac{\omega}{\omega \mp \omega_{cs}} \right) i E_x + \left(\frac{\omega}{\omega \mp \omega_{cs}} - \frac{\omega}{\omega \pm \omega_{cs}} \right) E_y \right] \tag{13}$$

$$\frac{i}{\varepsilon_0 \omega} j_z = -\sum_s \frac{\omega_{ps}^2}{\omega^2} E_z \tag{14}$$

where the $\pm$ symbol corresponds to the charge on the species being considered Equations (15)-(17) allow us to write $\boldsymbol{D}$ in terms of $\boldsymbol{E}$ and plasma parameters:

$$\begin{aligned} \varepsilon_0^{-1} D_x &= SE_x - iDE_y \\ \varepsilon_0^{-1} D_y &= iSE_x + DE_y \\ \varepsilon_0^{-1} D_z &= PE_z \end{aligned} \tag{15}$$

where we have used the following notation

$$R \equiv 1 - \sum_s \frac{\omega_{ps}^2}{\omega^2} \left(\frac{\omega}{\omega \pm \omega_{cs}} \right) \tag{15}$$

$$L \equiv 1 - \sum_s \frac{\omega_{ps}^2}{\omega^2} \left(\frac{\omega}{\omega \mp \omega_{cs}} \right) \tag{16}$$

$$S = \frac{1}{2}(R + L) \tag{17}$$

$$D = \frac{1}{2}(R - L) \tag{18}$$

$$P = 1 - \sum_s \frac{\omega_{ps}^2}{\omega^2} \tag{19}$$

Comparing Equation (15) and equation (3), gives us the following expression for the dielectric tensor:

$$\vec{\varepsilon} = \varepsilon_0 \begin{pmatrix} S & -iD & 0 \\ iD & S & 0 \\ 0 & 0 & P \end{pmatrix} \tag{20}$$

Now we must derive the wave equation from Maxwell's second and fourth equations:

$$\nabla \times \vec{E} = -\frac{\partial \vec{B}}{\partial t} \tag{21}$$

$$\nabla \times \vec{B} = \mu_0 \frac{\varepsilon}{\varepsilon_0} \frac{\partial \vec{E}}{\partial t} \tag{22}$$

where B is now associated with the waves. Substituting the curl of Equation (21) into equation (22) yields:

$$\nabla \times \nabla \times \vec{E} = -\frac{1}{c^2}\frac{\varepsilon}{\varepsilon_0}\cdot\frac{\partial^2 \vec{E}}{\partial t^2} \tag{23}$$

We are considering the propagation of waves. Therefore all quantities associated with the wave are of the form

$$e^{-i(k\cdot r-\omega\cdot t)} \tag{24}$$

where k is the magnitude of the propagation vector and r is the direction of propagation. Equation (23) becomes

$$\frac{c}{\omega}\vec{k}\times\left(\frac{c}{\omega}\vec{k}\times\vec{E}\right)+\frac{\varepsilon}{\varepsilon_0}\cdot\vec{E}=0 \tag{25}$$

where c is the speed of light. Define the following vector:

$$\vec{\mu}=\frac{c}{\omega}\vec{k} \tag{26}$$

By defining the plane of propagation such that $k_y = 0$, the components of μ are:

$$\mu_x = \mu\sin\theta \tag{27}$$

$$\mu_z = \mu\cos\theta \tag{28}$$

where θ is the angle between the propagation vector and the static magnetic field. Substituting Equation (20) into Equation (25), one finds

$$\vec{R}\cdot\vec{E} \equiv \begin{pmatrix} S-\mu^2\cos^2\theta & -iD & \mu^2\sin\theta\cos\theta \\ iD & S-\mu^2 & 0 \\ \mu^2\sin\theta\cos\theta & 0 & P-\mu^2\sin^2\theta \end{pmatrix}\begin{pmatrix} E_x \\ E_y \\ E_z \end{pmatrix} = 0 \tag{29}$$

For Equation (29) to be soluble, the determinant of this matrix must equal zero. Setting the determinant equal to zero will allow us to find an expression for θ. Algebra yields:

$$\sin^2\theta = \frac{-P\left(\mu^4 - 2S\mu^2 + RL\right)}{\mu^4(S-P)+\mu^2(PS-RL)} \tag{30}$$

And similarly:

$$\cos^2\theta = \frac{S\mu^4 - (PS+RL)\mu^2 + PRL}{\mu^4(S-P)+\mu^2(PS-RL)} \tag{31}$$

Dividing these results yields:

$$\tan^2\theta = -\frac{P\left(\mu^2-R\right)\left(\mu^2-L\right)}{\left(S\mu^2-RL\right)\left(\mu^2-P\right)} \tag{32}$$

Equation (32) contains the dispersion relation for the majority of waves that can propagate in a cold, magnetized plasma. Whistler waves, unbound R waves, propagate parallel to magnetic fields, *i.e.* $\theta = 0$. Equation (32) has three roots, P=0, L= μ^2 , and R= μ^2, corresponding to three different dispersion relations. A characteristic of the whistler wave is that it displays a resonance at the cyclotron frequency, *i.e.* $\boldsymbol{k}\rightarrow\infty$ as $\omega \rightarrow \omega_c$. This occurs in the third root, R= μ^2. As such the dispersion relation for the whistler wave is:

$$\left(\frac{c}{\omega}k\right)^2 = 1 - \frac{\omega_{ps}^2}{\omega^2}\left(\frac{\omega}{\omega-\omega_{cs}}\right) \tag{33}$$

Equation (33) indicates both high and low frequencies of propagation. However, whistler waves are those propagating below the cyclotron frequency. The distinction arises from the history of whistler wave mention earlier

3.2 Derivation of dispersion relation for waves traveling in cold bound plasma

The previous treatment of whistler waves provides insight into the nature of helicon waves; however it assumes that the wave is unbound. In the laboratory setting, one must account for the boundary conditions defined by the device.

Often laboratory devices are conductors, similar to wave guides. When electromagnetic waves propagate in a wave guide, it cannot be assumed that the direction of propagation is mutually perpendicular with the electric, and magnetic fields. For a cylindrical waveguide, the electric field is of the form:

$$\vec{E} = \vec{E}(r)e^{i(k_z z + m\theta - \omega t)} \tag{34}$$

where m is the mode of propagation and k_z is the magnitude of the propagation vector in the z-direction. In this case, derivatives can be written as

$$\begin{aligned} \frac{\partial}{\partial \theta} &\rightarrow im, \\ \frac{\partial}{\partial z} &\rightarrow ik_z, \\ \frac{\partial}{\partial t} &\rightarrow -i\omega, \end{aligned} \tag{35}$$

Using this, we can write Maxwell's 2nd and 4th Equations as

$$\nabla \times \vec{E} = i\omega \vec{B} \tag{36}$$

$$\nabla \times \vec{B} = -\frac{i\omega}{c^2} \vec{\varepsilon} \cdot \vec{E} \tag{37}$$

Equations (36) and (37) can be written in there components r ,θ, and z.

$$(\nabla \times E)_r = \frac{im}{r} E_z - ikE_\theta = i\omega B_r \tag{38}$$

$$(\nabla \times E)_\theta = ik_z E_r - \frac{d}{dr} E_z = i\omega B_\theta \tag{39}$$

$$(\nabla \times E)_z = \frac{1}{r}\frac{d}{dr}(rE_\theta) - \frac{im}{r} E_r = i\omega B_z \tag{40}$$

$$(\nabla \times B)_r = \frac{im}{r} B_z - ikB_\theta = -\frac{i}{\omega}(\kappa_1 E_r + \kappa_2 E_\theta) \tag{41}$$

$$(\nabla \times B)_\theta = k_z B_r - \frac{d}{dr} B_z = -\frac{i}{\omega}(-\kappa_2 E_r + \kappa_1 E_\theta) \tag{42}$$

$$(\nabla \times B)_z = \frac{1}{r}\frac{d}{dr}(rB_\theta) - \frac{im}{r} B_r = -\frac{i}{\omega}(\kappa_3 E_z) \tag{43}$$

where we introduce the notation:

$$\begin{aligned} \kappa_1 &= S\frac{c^2}{\omega^2}, \\ \kappa_2 &= -iD\frac{c^2}{\omega^2}, \\ \kappa_3 &= P\frac{c^2}{\omega^2} \end{aligned} \tag{44}$$

Equations (38) and (41) and can be solved for the transverse components of **E** to give:

$$\vec{E}_\perp = a\nabla_\perp E_z + b\nabla_\perp B_z + c\hat{e}_z \times \nabla_\perp E_z + d\hat{e}_z \times \nabla_\perp B_z \tag{45}$$

where the transverse gradient and electric field are defined as

$$\nabla_\perp = \nabla - \hat{e}_z \frac{\partial}{\partial z} \tag{46}$$

$$\vec{E}_\perp = \vec{E} - \hat{e}_z E_z \tag{47}$$

and the coefficients are:

$$
\begin{aligned}
a &= -\frac{ik_z\gamma}{\gamma^2+\kappa_2^2} \\
c &= \frac{ik_z\kappa_2}{\gamma^2+\kappa_2^2} \\
b &= \frac{i\omega\kappa_2}{\gamma^2+\kappa_2^2} \\
d &= \frac{i\omega\gamma}{\gamma^2+\kappa_2^2}
\end{aligned}
\tag{48}
$$

$$
\gamma = k_z^2 - \kappa_1 \tag{49}
$$

In a similar fashion equations (39) and (41) can be solved to give:

$$
\vec{B}_\perp = p\nabla_\perp E_z + a\nabla_\perp B_z + q\hat{e}_z \times \nabla_\perp E_z + c\hat{e}_z \times \nabla_\perp B_z \tag{50}
$$

where

$$
p = -\frac{ik_z^2\kappa_2}{\omega\left(\gamma^2+\kappa_2^2\right)} \tag{51}
$$

$$
q = -\frac{i\left(\kappa_1\gamma-\kappa_2^2\right)}{\omega\left(\gamma^2+\kappa_2^2\right)} \tag{52}
$$

Equations (45) and (50) can be substituted into the equations (40) and (43) to find :

$$
c\nabla_\perp^2 E_z + d\nabla_\perp^2 B_z - i\omega B_z = 0 \tag{53}
$$

$$
c\nabla_\perp^2 B_z + d\nabla_\perp^2 E_z - i\omega B_z = 0 \tag{54}
$$

Uncoupling Equations (53) and (54) yields

$$\left(c^2 - qd\right)\nabla_\perp^4 E_z + \left(iwq - \frac{id\kappa_3}{w}\right)\nabla_\perp^2 E_z - \kappa_3 E_z = 0 \tag{55}$$

$$\left(c^2 - qd\right)\nabla_\perp^4 B_z + \left(iwq - \frac{id\kappa_3}{w}\right)\nabla_\perp^2 B_z - \kappa_3 B_z = 0 \tag{56}$$

which can be recast as:

$$\left(\nabla_\perp^2 + \kappa_{\perp 1}^2\right)\left(\nabla_\perp^2 + \kappa_{\perp 2}^2\right)\begin{pmatrix} E_z \\ B_z \end{pmatrix} = 0 \tag{57}$$

where $\kappa^2_{\perp 1}$ and $\kappa^2_{\perp 2}$ are the roots to the equation

$$\left(c^2 - qd\right)k_\perp^4 - \left(i\omega q - \frac{id\kappa_3}{\omega}\right)k_\perp^2 - \kappa_3 = 0 \tag{58}$$

Solutions to the fourth order differential in Equation (57) are of the form

$$\Phi(r,\theta) = \sum_{m=-\infty}^{\infty} A_m J_m(k_\perp r) e^{im\theta} \tag{59}$$

where A_m is amplitude associated with the m[th] Bessel function. From equation (54), we note that *Ez* and *Bz* are proportional, i.e. $B_z = \Phi$, then $E_z = \alpha\Phi$. The z-components of the wave fields are then:

$$B_z(r,\theta,z,t) = \sum_{m=-\infty}^{\infty} A_m\left[J_m(k_{\perp 1} r) + \tau_m J_m\left(k_{\perp 2} r\right)\right] e^{i(k_z z + m\theta - \omega t)} \tag{60}$$

$$E_z(r,\theta,z,t) = \sum_{m=-\infty}^{\infty} A_m\left[\alpha_{1m} J_m(k_{\perp 1} r) + \alpha_{2m}\tau_m J_m\left(k_{\perp 2} r\right)\right] e^{i(k_z z + m\theta - \omega t)} \tag{61}$$

The constant τ_m is a factor to distinguish between the amplitudes of both Bessel functions. The values of α_1 and α_2 can be obtained from the roots of Equation (50) after substituting $B_z = \Phi$ and $E_z = \alpha\Phi$. This allows us to write $k_\perp$ in terms of α:

$$k_{\perp j}^2 = -\frac{i\omega}{d + \alpha_j c} \tag{62}$$

Equation (58) becomes:

$$\left(\gamma^2 + \kappa_2^2 + \gamma k_\perp^2\right)\kappa_3 + k_\perp^2\left[\kappa_1\left(\gamma + k_\perp^2\right) - \kappa_2^2\right] = 0 \tag{63}$$

The dispersion relation given by Equation (63) is identical to what was found for the unbound plasma, except that $k_\perp$ depends on the boundary conditions defined by the plasma device. Using Equations (57) and (58), we can find the other components of the electric wave fields:

$$E_{zm} = \frac{\omega\kappa_1 A_m}{k_\parallel \kappa_2 \kappa_3}\left[\beta_1 J_m(k_{\perp 1} r) + \tau_m \beta_2 J_m(k_{\perp 2} r)\right] \tag{64}$$

$$E_{rm} = \frac{i\omega A_m}{\kappa_2}\left[\delta_1 \frac{J_m'(k_{\perp 1} r)}{k_{\perp 1}} + \tau_m \frac{J_m'(k_{\perp 2} r)}{k_{\perp 2}}\right] - \frac{m\omega A_m}{r}\left[\frac{J_m(k_{\perp 1} r)}{k^2{}_{\perp 1}} + \tau_m \frac{J_m(k_{\perp 2} r)}{k^2{}_{\perp 2}}\right] \tag{65}$$

$$E_{\theta m} = -\frac{m\omega A_m}{r\kappa_2}\left[\delta_1 \frac{J_m(k_{\perp 1} r)}{k^2{}_{\perp 1}} + \tau_m \frac{J_m(k_{\perp 2} r)}{k^2{}_{\perp 2}}\right] - i\omega A_m\left[\frac{J_m'(k_{\perp 1} r)}{k_{\perp 1}} + \tau_m \frac{J_m'(k_{\perp 2} r)}{k_{\perp 2}}\right] \tag{66}$$

where j corresponds to the roots of equation (63) :

$$\begin{aligned} \beta_j &= \gamma - \frac{\kappa_2^2}{\kappa_1} + k_{\perp j}^2 \\ \delta_j &= \gamma + k_{\perp j}^2 \\ j &= 1,2 \end{aligned} \tag{67}$$

For a conducting metal wall, our boundary, condition is that the tangential components of $\boldsymbol{E}$ must go to zero. Applying this to equations (64) and (66), we find that at r = a:

$$\beta_1 J_m(k_{\perp 1}a) + \tau_m \beta_2 J_m(k_{\perp 2}a) = 0 \tag{68}$$

$$\frac{J'_m(k_{\perp 1}a)}{k_{\perp 1}} + \tau_m \frac{J'_m(k_{\perp 1}a)}{k_{\perp 2}} = \frac{im}{a\kappa_2}\left[\delta_1 \frac{J_m(k_{\perp 1}a)}{k_{\perp 1}^2} + \tau_m \delta_2 \frac{J_m(k_{\perp 2}a)}{k_{\perp 12}^2}\right] \tag{69}$$

Equations (64) and (66) can be added to eliminate τ_m and give:

$$\frac{im\delta_1}{k_{\perp 1}^2 a\kappa_2\beta_2} - \frac{1}{k_{\perp 1}\beta_1}\frac{J'_m(k_{\perp 1}a)}{J_m(k_{\perp 1}a)} = \frac{im\delta_2}{k_{\perp 2}^2 a\kappa_2\beta_2} - \frac{1}{k_{\perp 2}\beta_2}\frac{J'_m(k_{\perp 2}a)}{J_m(k_{\perp 2}a)} \tag{70}$$

By solving this transcendental equation, we can find values for $k_{\perp 1}$ and $k_{\perp 2}$ which can be placed back into equation (61) to construct the theoretical wave fields.

Chapter 4

Construction and design of a Plasma chamber

Laboratory studies of plasmas necessitate the construction of a chamber in which the conditions needed for ignition can be created. One must have a region of low pressure in which energy can be transferred to the gas. In the following chapter, we descried the plasma device that is under construction at IWU, seen in Figure 2. The discussion will include the plasma chamber, and the vacuum system.

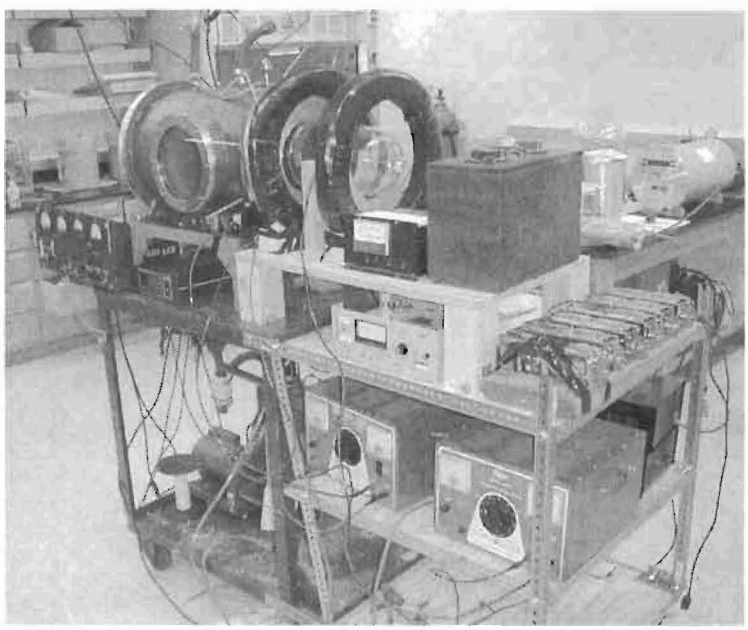

Figure 2:The I.W.U. Plasma Device

4.1 Plasma Chamber

The plasma chamber is a steel cylinder with a length of 0.61m and radius of 0.18m and a glass bell jar. The chamber has an approximate volume of 6.4×10^{-2} m^3. The chamber has geometry similar to the waveguide we assumed in section 2. This means the dispersion relation and waveforms found earlier should be seen in our experimental device.

4.2 Vacuum System

When a gas is ionized an electron is liberated from an atom. If this electron recombines with this an ion, photons are released. Continuous recombination creates the glow of a plasma. If the rate of recombination is greater than the rate of ionization the plasma will return to the gas state. The amount of energy required to maintain a plasma depends on the number of atoms present in the chamber. Typically, experiments are performed at pressures of 10^{-3} Torr. However, a base pressure of 10^{-6} Torr is needed to insure the purity of the gas being ionized. To create this high vacuum, we have assembled a vacuum system shown schematically in Figure 3 consisting of a mechanical roughing pump, and a diffusion pump.

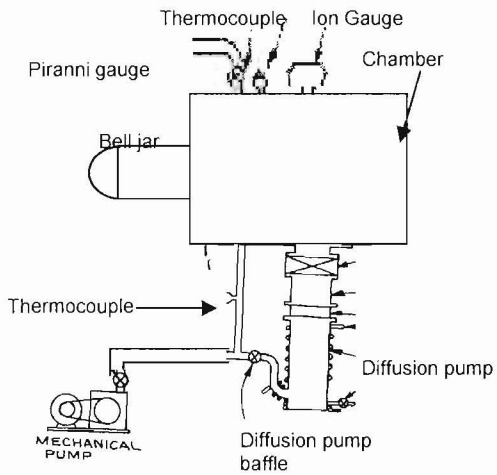

Figure 3: A Schematic of the Vacuum Chamber, including diffusion pump, mechanical pump, and gauges

4.2.1 Roughing Pump

A mechanical roughing pump is one of the most common types of vacuum pumps. While there are many different varieties, the basic principles of operation are the same. A cross section of a two-vane rotary pump is seen in Figure 4.

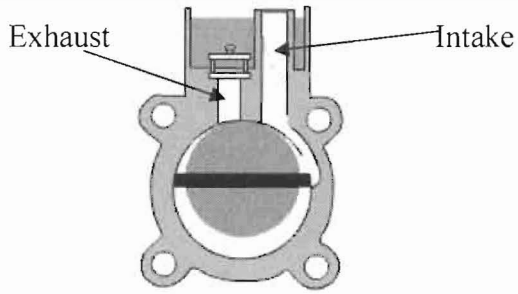

Figure 4: Cross Section of Two-vane rotary pump

This pump contains an offset steel wheel. Mounted in the wheel is a pair of spring loaded metal vanes, which are in constant contact with the inner walls of the pump. The casing of the pump is then filled with vacuum oil, which serves to lubricate the wheel and form the seal between the casing and the vanes. As the wheel rotates, first vane passes the intake valve and opens a volume to the chamber. This volume expands as the wheel rotates and causes an area of low pressure within the pump, pulling gas molecules form the chamber. As the second vane comes around it closes this volume to the chamber. The asymmetric motion of the wheel causes this volume of gas to be compressed, forced through the pump oil, and out the exhaust.

In our experiment the Welch **DUOSEAL**® 1400B is used. This has a pump rate of 25 L/min, and an ultimate pressure of 10^{-4} Torr. We have observed a mechanical pump limit of 10^{-2} Torr. This is likely due to impure pump oil.

4.2.2 Diffusion pump

To reach the desired base pressure, a diffusion pump is used. A cross section a diffusion pump is shown in Figure 5.

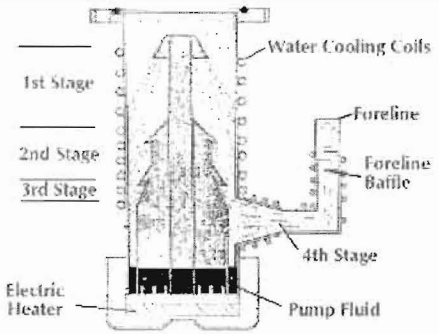

Figure 5: Cross Section Diffusion Pump

Diffusion pumps are low pressure pumps that work on the principle of convection. The base of a diffusion pump contains an electric heater, which vaporizes a liquid reservoir of organic oil that consists of large hydrocarbons. Once the oil is in a vapor form, it begins to rise. It is then deflected downward towards the water cooled walls of the pump body. As the oil vapor moves toward the walls, it collides with molecules in the pump volume. Momentum exchange forces particles downward, creating a pressure gradient within the pump. This pressure difference pulls molecules from the chamber to foreline, where the a mechanical pump removes these molecules from the chamber. The diffusion doesn't actually eliminate any gas from the volume; it redirects particles, allowing the mechanical pump to work at low pressures. Eventually the oil vapor will make contact with the water cooled walls of the pump and condenses back into reservoir. Diffusion pumps can operate over a range of 10^{-1} -10^{-7} Torr.

One of the major concerns when using a diffusion pump is that they can't operated above 10^{-1} Torr. If the diffusion pump oil is in vapor form and vented to atmosphere it can be catastrophic to an experiment. At high pressures the mean free path of the particles becomes much less than that of the trip to the cooled walls. At high pressures hydrocarbons diffuse into the chamber where they will then oxidize, coating one's experimental apparatus with tar.

Our chamber uses a **VEECO®** EP-4W diffusion pump. It has a top pump rate 425 L/sec. Currently, our chamber is able to achieve pressures of $5x10^{-3}$ Torr. A lower base pressure of 10^{-6} Torr is desirable; however a leak in the system makes this currently unattainable.

4.3 Vacuum Gauges

Measuring pressures near atmosphere is a fairly simple task. However, as the pressure decreases, it becomes increasing difficult to make measurement using conventional means. To measure low pressures, we use a variety of gauges that utilize some of the properties of a gas.

4.3.1 Thermal Conductivity Gauges

As the pressure of a gas decreases, the thermal-conductivity of the gas also decreases because there are fewer particles in contact with a warm surface to conduct heat away from a hot source. An entire class of thermal conductivity gauges are based on this principle, including the thermocouple and the Pirani gauge.

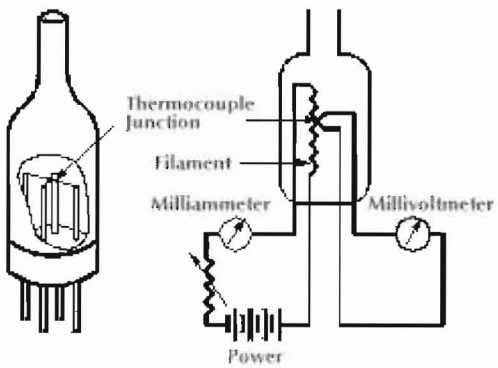

Figure 6: A Circuit Diagram of a Thermocouple gauge

A thermocouple, seen in Figure 6, contains a heater filament and a wire held at constant current. As pressure in the gauge decreases, the temperature of the wire increases casuing its resistance to increase. This change in resistance can be measured as a change in voltage across the wire. Thermocouples can operated over any pressure range, but are only accurate down to 10^{-3} Torr. These gauges are often used because they are rugged and simple in design. We use this gauge to measure our Foreline pressure

The Pirani gauge, seen in Figure 7 gauge works on the same principle. To measure a change in resistances, use a sensitive bridge circuit. The bridge circuit allows one to measure smaller variations in resistance, eliminating the need for a heating element. We use the Pirani to measure chamber pressure.

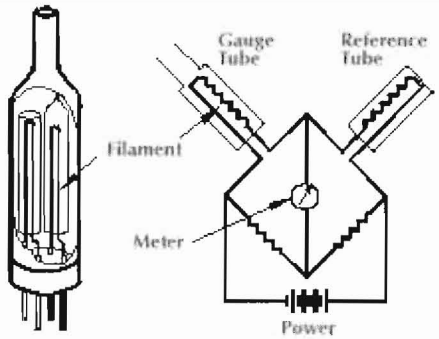

Figure 7: A Diagram of the bridge circuit in a Pirani gauge

4.3.2 Hot Ionization Gauges

As pressures drop below 10^{-3} Torr it is necessary to use an ionization gauge to measure the pressure.

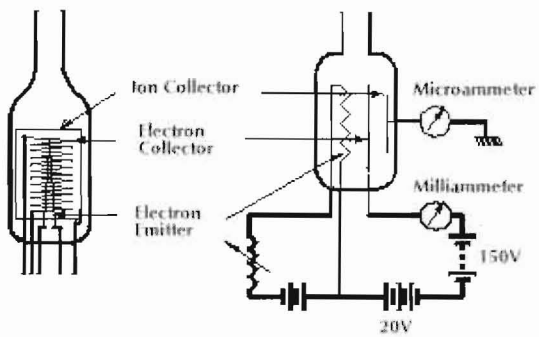

Figure 8: Ionization Gauge

In a hot ionization gauge, shown in Figure 8, electrons are liberated from a heated emitter filament and accelerated through a potential difference to an anode . As electrons are accelerated through the gas in the gauge, they collide with atoms and ionize them. The ions are then collected at a negatively biased wire. The number of ions collected can be measured as a current. This current is proportional to the number of atoms and hence the pressure in the gauge. Ion gauges can be used between 10^{-3} and 10^{-9} Torr. Above 10^{-3} Torr electrons collide too often with the gas and the collector current is to large. Additionally, at high pressures the emitter will burnout, much like a light bulb. As pressures reach 10^{-9} Torr, X-rays are emitted as electron

strike the anode. These X-rays cause photoelectric effect on metal pieces within the gauge and place a low pressure limit on ion gauges. Our chamber uses an NRC 501 triode gauge as the principle low pressure gauge.

4.3.3 Cold Cathode Gauges

A cold cathode or Penning gauge, seen in figure 9, works on similar principle as an ion gauge, but they do not use heated filaments for the production of electrons.

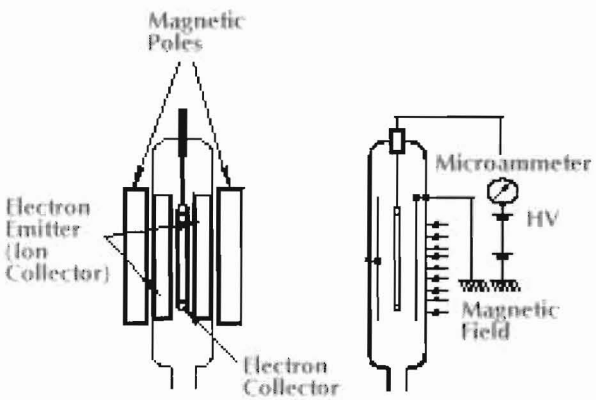

Figure 9: Penning Gauge

The cathodes are located on either side of an anode, in a region of magnetic field. As electrons are emitted, they are accelerated towards the anode. Due to the magnetic field the electrons travel in helix, increasing the path an electron takes through the gas. If the electron is not collected at the anode it continues, toward the opposing cathode, slowing and eventually changing direction. In this way a single electron can make many passes through a gas before being collected. During these passes, the electron is ionizing the gas in the gauge. Since one electron can cause much more ionization then those is a hot cathode gauge, the number of electrons needed is much less, and there is no need for a hot cathode to produce many electrons. Our Penning gauge is used as a low pressure gauge.

Chapter 5

The Source

The plasma source depicted in Figure 10 is used to ionize our gas.

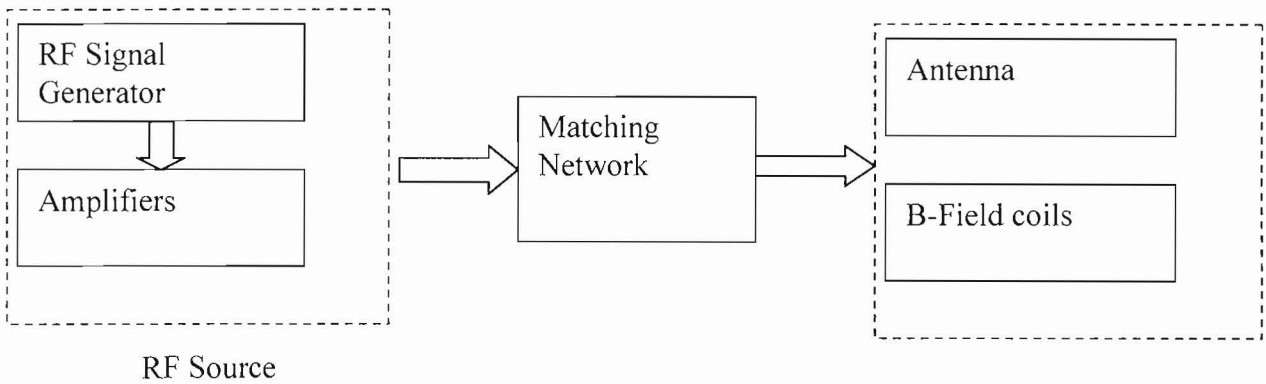

Figure 10: A flow diagram of the plasma source. The RF source creates a signal which is feed to the antenna through a matching network for maximum power transfer. The antenna is in a region of magnetic field

5.1 Amplifiers

The 10 dB signal from the RF generator is not strong enough ionize the plasma volume and has to be amplified. The RF signal is first fed into a power amplifier [16]. This amplifier operates from 1.6-30 MHz with an output power of 20W. The signal from the first amplifier is then fed into a 300W amplifier with an operating range of 2-30 MHz [17], see appendix II.

5.2 Matching Circuit

The power available to this device, <300W, is modest. As such, care must be taken to insure that maximum power reaches the antenna. The amplifiers have an output impedance of 50 Ω, while the antenna has a resistance of 0.18 ohms and an inductance of 6μH. This results in an impedance mismatch on the order of 50 Ω when at our desired operating frequency of f = 13.5MHz. This mismatch will result in much of the power being reflected at the antenna.

As a result little power would be available to ionize the gas, and the reflected power would destroy the amplifiers. To avoid this problem we have constructed a matching network. Figure 11 depicts the circuit diagram of the plasma source.

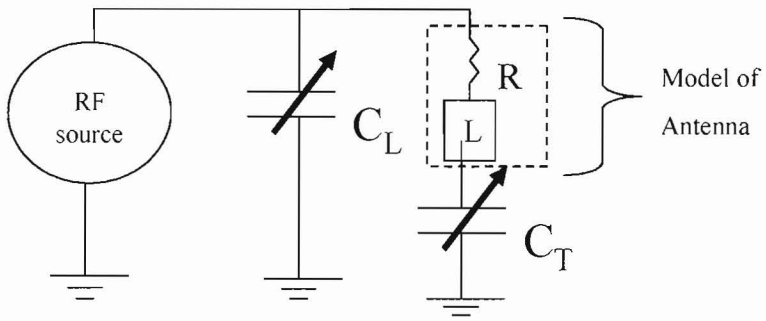

Figure 11: Circuit diagram of the Plasma source. The antenna is modeled as an inductor and resistor in series. The capacitors C_L and C_T are variable capacitors that match the output impedance of the source and antenna. R, L, and C_T are the tuning arm of the network and C_L is the load arm

5.2.1: Conditions for Impedance Matching

The total impedance of the tuning arm is

$$Z_t = i\omega L - \frac{1}{i\omega C_T} + R \tag{71}$$

where R is the antenna resistance, L is the inductance of the antenna., ω is the angular frequency of the signal and C_T is a tuning capacitor. Let us define the quantity:

$$L^* = L\omega - \frac{1}{\omega C_T} \tag{72}$$

The admittance of the tuning arm is:

$$Y_t = \frac{1}{Z_t} = \frac{1}{iL^* + R} \tag{73}$$

The total admittance of the tuning arm and the load capacitor is:

$$Y = Y_L + Y_t = \frac{R}{R^2 + L^{*2}} - i\left[\frac{L^*}{R^2 + L^{*2}} - \omega C_L\right] \tag{74}$$

Maximum power transfer occurs when the output impedance, of the RF amplifier z, equals the impedance of the tuning and load arms:

$$Z = \frac{R}{R^2 + L^{*2}} - i\left[\frac{L^*}{R^2 + L^{*2}} - \omega C_L\right]^{-1} \tag{75}$$

By equating the imaginary and real portions of equation (75), we can find an expression for the tuning and load capacitor:

$$Z = \left[\frac{R}{R^2 + L^{*2}}\right]^{-1} \tag{76}$$

$$\omega C_L = \frac{L^*}{R^2 + L^{*2}} \tag{77}$$

From Equation (76) and (77), we find an expression for the load capacitance

$$C_L = \frac{L^*}{RZ\omega} \tag{78}$$

The resistance of the antenna is significantly lower than the output impedance of the source. In the limit of $Z >> R$ Equation (76) reduces to:

$$L^* = \sqrt{RZ} \tag{79}$$

Substituting this result into Equation (78) , we find the load capacitance needed for impedance matching

$$C_L = \frac{1}{\omega\sqrt{RZ}} \tag{80}$$

Substituting Equation (80) into Equation (76) yields:

$$L\omega - \frac{1}{\omega C_T} = \sqrt{RZ} \tag{81}$$

From this we find an expression for the tuning capacitor

$$C_T = \frac{1}{\omega^2 L - \omega\sqrt{RZ}} \tag{82}$$

Equations (80) and (82) indicate the capacitance needed for impedance matching as a function of frequency. Figure 11 is a plot of matching capacitance verses frequency.

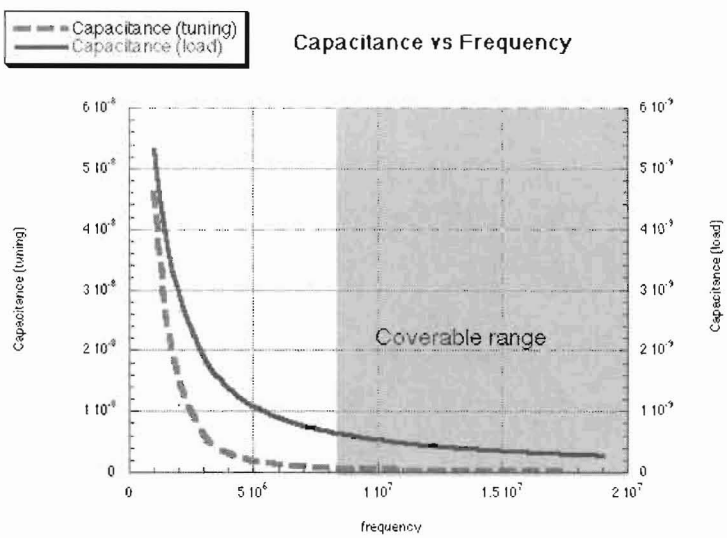

Figure 12: Matching Capacitance as a function of Frequency coverable range is f > 8MHz

C_T is a pair of air filled variable capacitors wired in parallel, with a range of 0.18nF-6.15nF. C_L is a set of six variable air filled capacitors wired in series, with a range of 0.02nF-0.07nF. This arrangement allows us to transmit maximum power to the antenna at frequencies in the gray region in Figure 12.

5.3: The Antenna

Our device uses helicon waves as a plasma source. To create these helicon waves, an antenna is used. The geometry of the antenna determines the helicon modes that are exited. Certain antennas designs can excite modes that destructively interfere, resulting in low density plasmas, while other antenna designs excite only one mode resulting in much higher plasma densities. The antenna best suited for our needs is the Nagoya Type III [8].

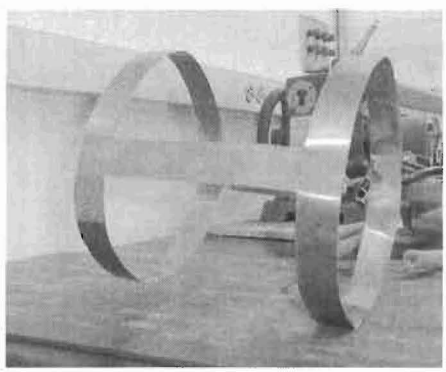

Figure 13: The Nagoya Type III antenna used to launch the Helicon wave

The Nagoya Type III, shown in Figure 12, has been shown to primarily excite the m = +1 mode, with fairly good densities [9]. In addition efficiency, the Nagoya Type III has a simple design and was easy to construct. The antenna was cut from 0.24mm copper sheeting, and silver soldered to fit the dimensions of the bell jar mounted on the end of the chamber. High power transmission lines were made from 3/8'' copper tubing.

5.4: Magnetic Field coils

There are many waves that can propagate in plasma. However, only a select few do so in an unmagnetized plasma. Since helicon waves can only propagate in a magnetized plasma, the source must be placed in a region of magnetic field. A fairly uniform field is needed to avoid many of the particle drifts associate with curvature in field lines. These fields are generated by a pair of concentric field coils.

The coils are made of 110 turns 10 and 8 AWG wire wrapped on iron rings. The coils can carry 20A. This arrangement produces the on axis field shown in Figure 13. The magnetic field over the antenna region varies 7% about the maximum, with a peak value of 75 Gauss.

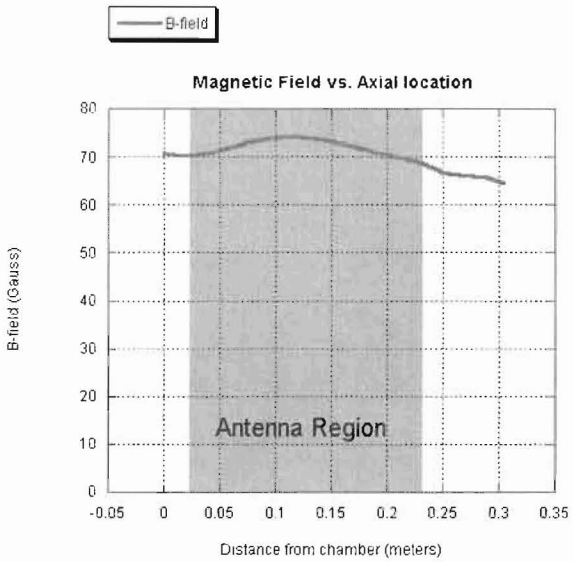

Figure 14:Magnetic field over Antenna region

The field strength is satisfactory, but efforts have been made to reduce the 7% variation. One concern is that the antenna doesn't sit in the center of the coils. To try and compensate for this a third coil, 30 turns, was wired separately and placed on the chamber. This coil was didn't have strong affect on the shape of the field.

Chapter 6

Diagnostics

There are many types of diagnostic that can be use to extract information from our plasma. For our initial studies, we plan to make use of two standard plasma diagnostics the Langmuir probe and the B-dot probe.

6.1: The Langmuir probe

The Langmuir probe is a simple diagnostic that has been used for roughly 50 years. This probe allows us to measure the ion density n_i, the electron density, n_e, the electron temperature kT_e, and the electron distribution function [5]. Langmuir probes are very durable, and respond quickly to changes in the plasma; however they do perturb the plasma and could be problematic to certain experiments. The length scale associated with this perturbation is the Deye length:

$$\lambda_D \equiv \left(\frac{\varepsilon_0 kT_e}{ne^2} \right)^{1/2} \tag{83}$$

Placeing values for helicon plasma into equation (83) the Debye length $10^{-3.5}$m. This is significantly less than our indicated resolution and length scales associated with intended studies. As such, Langmuir probe will have a negligible effect.

Physically, the Langmuir probe is a small metal tip, which is inserted into the plasma [8]. The surface area of the tip is typically on the order of 10^{-6} m^3. A cylindrical tip is commonly used however; disks and spherical geometry are also options. Once in the plasma, a bias is applied to the probe, which establishes a potential in the plasma. Ions and electrons will be collected, depending on their kinetic energy. Typically one ramps the bias from a negative voltage to a positive voltage (see appendix I), allowing one to measure the distribution function by the current that is collected by the probe. By plotting the probe current as function of the probe voltage, one obtains a langmuir trace from which information about the plasma can be extracted.

If multiply equation (1) for current density by the surface area of probe we find:

$$I = A\sum_{s} n_s q_s \bar{v}_s \tag{84}$$

where A is the surface area of the tip and I is the total current recorded from the probe. The velocity vs in equation (84) is now the average particle given by the first moment of the distribution function:

$$\bar{v}_s = \frac{1}{n}\int v f_s(\vec{v}) d\vec{v} \tag{85}$$

If we consider particle velocity in only the x direction, we can combine Equations (84) and (85) to give:

$$I = nqA \int_{v_{\min}}^{\infty} v_x f(v_x) dv_x \tag{86}$$

The Langmuir probe collects particles with enough energy to over-come the potential of the probe bias. Energy considerations allow us to change our integration variable:

$$qV = \frac{1}{2}mv^2 \Rightarrow d(qV) = mvdv \tag{87}$$

where V is the bias applied to the probe and m is the mass of an electron. Substituting this result into equation (86) gives:

$$I = \frac{nqA}{m_e}\int_{qV}^{\infty} f(qV) d(qV) \tag{88}$$

Taking the derivative of the measure current with respect to the bias yields:

$$\frac{dI}{d(qV)} \alpha\, f(qv) \tag{89}$$

From Equation (85) one can reproduce the velocity distribution function of the plasma.

Due to the redistribution of velocities via equpartition theorem often the velocity distribution is Maxwellian. Maxwellian distributions are of the form:

$$f_e(\vec{v}) = n\left(\frac{2\pi kT_e}{m_e}\right)^{-3/2} \exp\left(\frac{-\frac{1}{2}m_e|\vec{v}|^2}{kT_e}\right) \tag{90}$$

The probe trace of a plasma with a Maxwellian velocity distribution is shown in Figure 15:

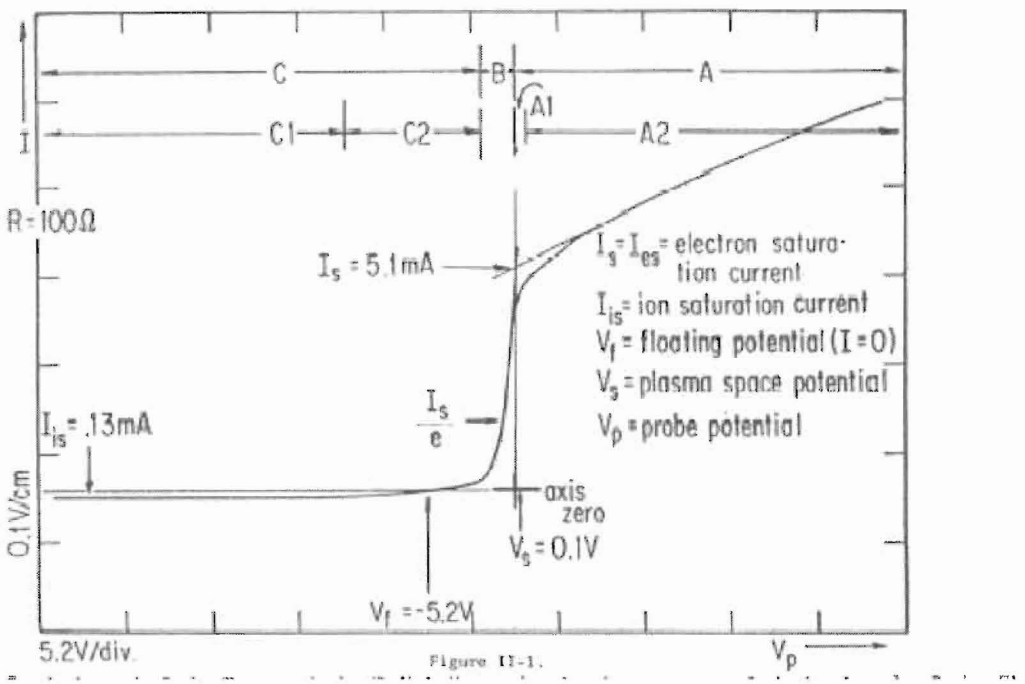

Figure 15: Typical Langmuir Trace for a plasma with a Maxwellian speed distribution

This is the distribution we will assume from here on. Substituting equation (90) into (86) gives us the probe current due to particles moving in the x direction

$$I(\vec{v}) = nqA\int_{v_{min}}^{\infty} dv_x v_x \left(\frac{2\pi kT_e}{m_e}\right)^{-3/2} \exp\left(\frac{-\frac{1}{2}m_e|\vec{v}|^2}{kT_e}\right) \tag{91}$$

Region C in Figure 15 corresponds to a large negative bias applied to the probe. In this region all the ions near the probe tip are collected. This is referred to as the ion saturation current. To find the saturation current the tip voltage must negative enough to repel the electrons or:

$$eV = kT_e \tag{92}$$

This potential is also the voltage at which the electrons are being collected, which is significantly higher then the thermal energy of the ions. We can then write the ion saturation current as:

$$I_{is} = neA\left(\frac{2kT_e}{m_i}\right)^{\frac{1}{2}} \tag{93}$$

As the probe bias increases electrons with enough energy to overcome the potential are also collected. The total current collected then is the difference of the saturation current and the current due to high speed electrons:

$$I(v) = I_{is} - neA\int_{v_{min}}^{\infty} dv_x v_x \left(\frac{2\pi kT_e}{m_e}\right)^{\frac{-1}{2}} \exp\left(\frac{-\frac{1}{2}m_e v_x^{\,2}}{kT_e}\right) \tag{94}$$

substituting equation (83) into equation (90) and integrating yields

$$I(v) = I_{is} - neA\left(\frac{kT_e}{2\pi m_e}\right)^{\frac{1}{2}} \exp\left(\frac{eV}{kT_e}\right) \tag{95}$$

Since I_{is} is proportional to the reciprocal of the ions mass we can take the limit $I_{is} << I$ giving us

$$I(v) \cong -neA\left(\frac{kT_e}{2\pi m_e}\right)^{\frac{1}{2}} \exp\left(\frac{eV}{kT_e}\right) \tag{96}$$

If we take the natural log of equation (92) and then differentiate with respect to **V** we find:

$$\frac{d\ln|(I)|}{dV} = \frac{e}{kT_e} \tag{97}$$

From this we can then extract the electron temperature. We can also substitute this value back into equation (92) along with the electron saturation current and in this way find the electron number density.

6.2: B-dot probe

To measure time varying magnetic fields within the plasma a magnetic fluctuation, or B-dot, probe is used [7]. The actual probe is a small coil of wires, oriented such that wire loops are axial to the field component being measured. The time varying magnetic field will induce voltage in the coils given by Faraday's Law:

$$V = NA\frac{dB(t)}{dt} \tag{98}$$

where N is the number of turns in the probe and A is the coil area. This probe measures the time rate change of magnetic field. This measurement can be feed through an integrator (see appendix I) to reconstruct the magnetic fields.

6.4: DAQ card/LabVIEW

The voltages from both probes will be conditioned and digitized for later analysis using a 16-bit data acquisition card with eight differential inputs though the DAQ interface shown in Figure 16.

Figure 16: The DAQ Card Interface

The DAQ card is controlled by software written in LabVIEW[10]. LabVIEW programs will read both the probe current and the probe bias from the Langmuir probe and perform the calculations mentioned earlier to extract the desired plasma parameters [10].

Chapter 7

Future Work and Conclusions

7.1: Work remaining

The current status of the chamber is that much remains to done. The next important step is the completion and testing of the power amplifiers. If the amps are found to meet our power requirements, they will then be connected to the RF generator and the matching circuit to complete the source.

Work is still needed on the vacuum system to reach the desired base pressure of 10^{-6} Torr. This entails using leak detecting techniques to find the chambers faulty seal. A vacuum system of this size has a number of O-rings and gaskets that when cracked or dry could cause leaks. Since the system leak is so small, it may take considerable time to find the leak.

Once a suitable base pressure is reached, the chamber will be filled with argon to an operating pressure of 10^{-3} Torr and an argon plasma will be create. Though any gas can be ionized to create a plasma, argon is well suited for our needs. Argon is an inert gas which makes it neither corrosive nor explosive. Non-inert gases could potentially oxidize, coat the chamber wall, or ruin the pump oils. Gases exhausted through roughing are subject to high pressures and temperatures. Reactive gases could potentially explode under these conditions. Argon also has a reasonably low first ionization energy of about 15.75eV.

It will also be important to magnetize the entire plasma volume. The dispersion relation for the bound helicon assumed the boundary to be a conductor, which meant the electric fields went to zero. However our current apparatus only has a magnetic field in the antenna region. Since the helicon waves need magnetic fields to propagate, they will only be present in the source. The walls of the bell jar are a dielectric, which means our boundary conditions don't necessarily apply. If the chamber body was wrapped with wire we could generate a magnetic field, and wave fields could be measured as calculated. Magnetizing the plasma volume would also allow us to do wider variety of experiments.

7. 2: Purposed experiment

When helicon plasma sources are used in the laboratory, there have been three distinct modes of operation documented [6]. In the capacitive mode, or E mode, high voltages on the antenna ionize particles by transferring energy through plasma sheaths [6]. This mode is characterized by low number densities and a high plasma potential. A distinct transition can be seen between the capacitive mode and the inductive mode, or H mode, marked by a density jump and a drop in the plasma potential. Recent experiments showed that as rf power increases the antenna creates azimuthal electric fields [6]. If the source is operating a frequency below the plasma frequency then these electric fields are evanescent. It was also shown that the skin depth corresponds directly to the transition between modes. The third mode observed is the helicon mode, or W mode. This is the mode where helicon waves are exited and propagate through the plasma. This mode exhibits much higher densities than the other modes. Kaeppelin *et al.* were able to show that this transition depends directly on the plasma density as opposed to the actual RF power [6].

Our plasma chamber could be used further investigate the behavior of the inductive mode near and above the plasma frequency. We could also investigate the density dependence of both the E-H and the H-W mode transitions. Further understanding of the characteristics could lead to better control of plasma parameters, as well as an understanding of helicon wave plasma production.

Bibliography

1. Chen, Francis F., *Introduction to plasma physics and controlled Fusion 2nd ed.* , Plenum Press 1984
2. Swanson, D.G., *Plasma Waves,* Academic Press Inc. 1989
3. Schneider, Darryn A., Helicon Waves in High density plasmas, Doctorial thesis Australian National University
4. National Research Council, *Plasma Science,* National Academy Press, 1995
5. Wong, A.Y. *Introduction to Experimental Plasma Physics,*UCLA report, 1977.
6. V. Kaeppelin, M.Carrere and J.B Faure, *Different operational regimes in a helicon scource,*Review of Scientific Instruments 72 (12) 2001.
7. Keiter, Paul A., *Experimental Investigation of Ion Temperature Anisotropy Driven Instabilities in a High Beta Plasma, Doctorial thesis*, West Virgina University, 1999
8. Balkey, Matthew M., *Optimization of a Helicon Plasma Source for Maximum Density with Minimal Ion Heating, Doctorial thesis*, West Virgina University, 2000
9. Kamenski, I.V., Borg, G.G., "An evaluation of different antenna designs for helicon wave exitation n cylindrical plasma source" Phys. Plasmas 3 (12) Dec 1996
10. Mores, Mike, *Development of a Data Acquisition and Analysis System for Plasma Diagnostics*, Reseach Honors thesis Illinois Wesleyan University, 2002
11. Fuchs. Ursi, proceedings of the 12th general assembly: 1957. Reported by Dr. Fuchs in discussion
12. P. Aigrain. Les Helicons dans le Semiconducteurs. IN *Proceedings: International Conference on Semiconductor Physics*, page 224, Prague, 1960. Publishing House of the Czechoslovak Academy of Sciences.
13. R.M. Gallet, J.M. Richardson, B. Wieder, G.D. Ward, and G.N. Harding. Microwave Whistler Mode Propagation in a Dense Laboratory Plasma. *Phys. Rev. Lett.*,4(7):347, 1960.
14. R.W. Boswell. Plasma Production using a Standing Helicon Wave. *Phys. Lett.*, 33A(7):457, 1970.
15. R.W. Boswell and Henry. Pulsed High Rate Plasma Etching with Variabke Si/SiO_2 Selectivity and Variable Si Etch Profiles. *Appl. Phys. Lett.*, 47(10):1095, 1985
16. Application note AN-779, Motorola Semiconductor Products
17. Granberg, Helge, *EB-27A Engineering Bulletin,* Motorola, 1980.
18. Hansen, S, *Some Resources and Ideas for Plasma Experiments, the* Bell Jar 4 (2) 1997

Appendix I: Circuits

Figure 1 - Langmuir Probe Experiment

Left: Circuit Schematic; Right: Characteristic Curve

(After R. Jones course notes)

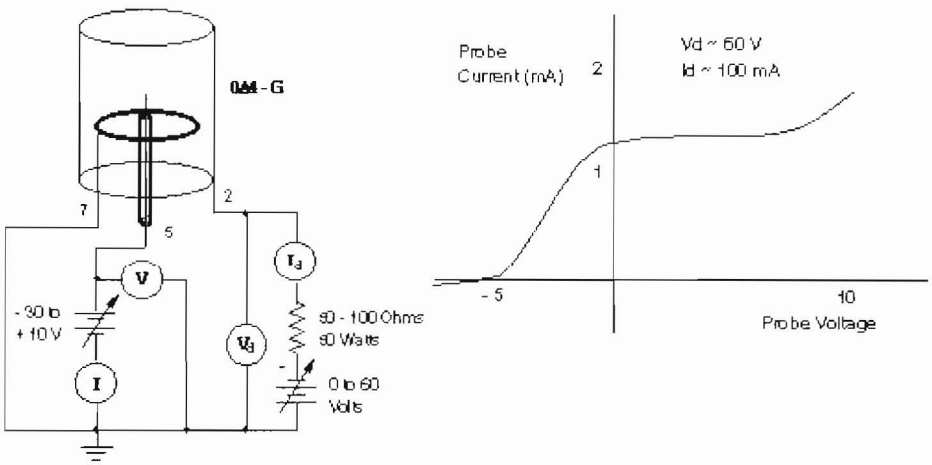

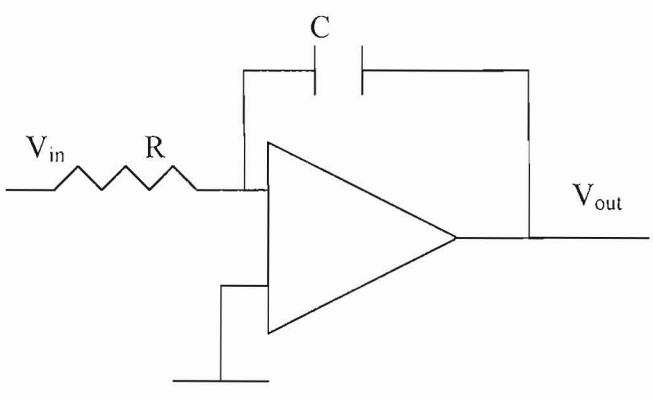

Figure 1: A Simple Integrator Circuit

Appendix II: Amplifier Specifications

AN-779
Application Note

LOW-DISTORTION 1.6 TO 30 MHz SSB DRIVER DESIGNS

Prepared by
Helge O. Granberg
RF Circuits Engineering

A general discussion for broadband drivers and their requirements for linear operation. Design examples are given using Motorola plastic transistors and high-gain hybrid modules designed for operation in the 1.0 to 250 MHz range. The amplifiers range in power gain from 25 to 55 dB and are capable of driving power amplifiers to levels up to several hundred watts.

MOTOROLA Semiconductor Products Inc.

LOW-DISTORTION 1.6 TO 30 MHz SSB DRIVER DESIGNS

GENERAL CONSIDERATION

Two of the most important factors to be considered in broadband linear amplifier design are the distortion and the output harmonic rejection.

The major cause for intermodulation distortion is amplitude nonlinearity in the active element. The nonlinearity generates harmonics, and the fundamental odd-order products are defined as $2f1-f2$, $2f2-f1$, $3f2-2f2$, $3f2-2f1$, etc., when a two-tone test signal is used. These harmonics may not always appear in the amplifier output due to filtering and cancellation effects, but are generated within the active device. The amplitude and harmonic distortion cannot really be distinguished, except in a case of a cascaded system, where even-order products in each stage can produce odd-order products through mixing processes that fall in the fundamental region.[2] This, combined with phase distortion—which in practical circuits is more apparent at higher frequencies—can make the distortion analysis extremely difficult;[5,2] whereas, if only amplitude distortion was present, the effect of IMD in each stage could easily be calculated.

In order to expect a low harmonic output of the power amplifier, it is also important for the driving source to be harmonic-free. This is difficult in a four-octave bandwidth system, even at 10-20 watt power levels. Class A biasing helps the situation, and Class A push-pull yields even better results due to the automatic rejection of even harmonics.

Depending on the application, a full Class A system is not always feasible because of its low efficiency. The theoretical maximum is 50%, but practical figures are not higher than 25% to 35%. It is sometimes advantageous to select a bias point somewhere between Class AB and A which would give sufficiently good results, since filtering is required in the power amplifier output in most instances anyway.

In order to withstand the high level of steady dc bias current, Class A requires a much larger transistor die than Class B or AB for a specific power output. There are sophisticated methods such as generating the bias voltage from rectified RF input power, making the dc bias proportional to the drive level.[1] This also yields to a better efficiency.

20 W, 25 dB AMPLIFIER WITH LOW-COST PLASTIC DEVICES

The amplifier described here provides a total power gain of about 25 dB, and the construction technique allows the use of inexpensive components throughout. The plastic RF power transistors, MRF475 and MRF476, featured in this amplifier, were initially developed for the CB market. The high manufacturing volume of these TO-220 packaged parts makes them ideal for applications up to 50 MHz, where low cost is an important factor.

The MRF476 is specified as a 3-watt device and the MRF475 has an output power of 12 watts. Both are extremely tolerant to overdrive and load mismatches, even under CW conditions. Typical IMD numbers are better than -35 dB, and power gains are 18 dB and 12 dB, respectively, at 30 MHz.

The collectors of the transistors are electrically connected to the TO-220 package mounting tab which must be isolated from the ground with proper mounting hardware (TO-220 AB) or by floating heat dissipators. The latter method, employing Thermalloy 6107 and 6106 heat dissipators, was adapted for this design. Without an airflow, the 6106 and 6107 provide sufficient heat sinking for about 30% duty cycle in the CW mode. Collector idle currents of 20 mA are recommended for both devices, but they were increased to 100 mA for the MRF475 and to 40 mA for the MRF476 to reduce the higher order IMD products and to achieve better harmonic suppression.

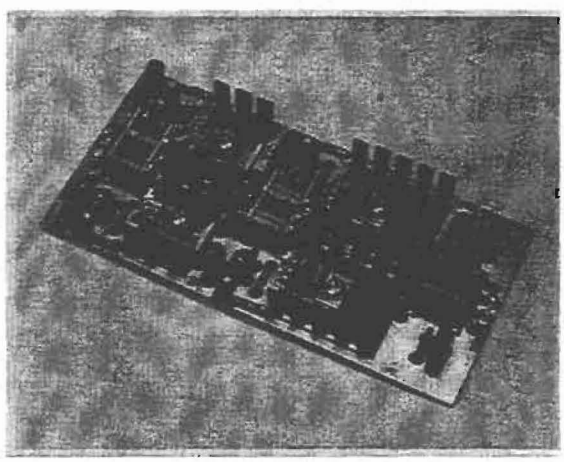

FIGURE 1

Biasing and Feedback

The biasing is achieved with the well-known clamping diode arrangement (Figure 2). Each stage has it own diode, resistor, and bypass network, and the diodes are mounted between the heat dissipators, being in physical contact with them for temperature-tracking purposes. A better thermal contact is achieved through the use of silicone grease in these junctions.

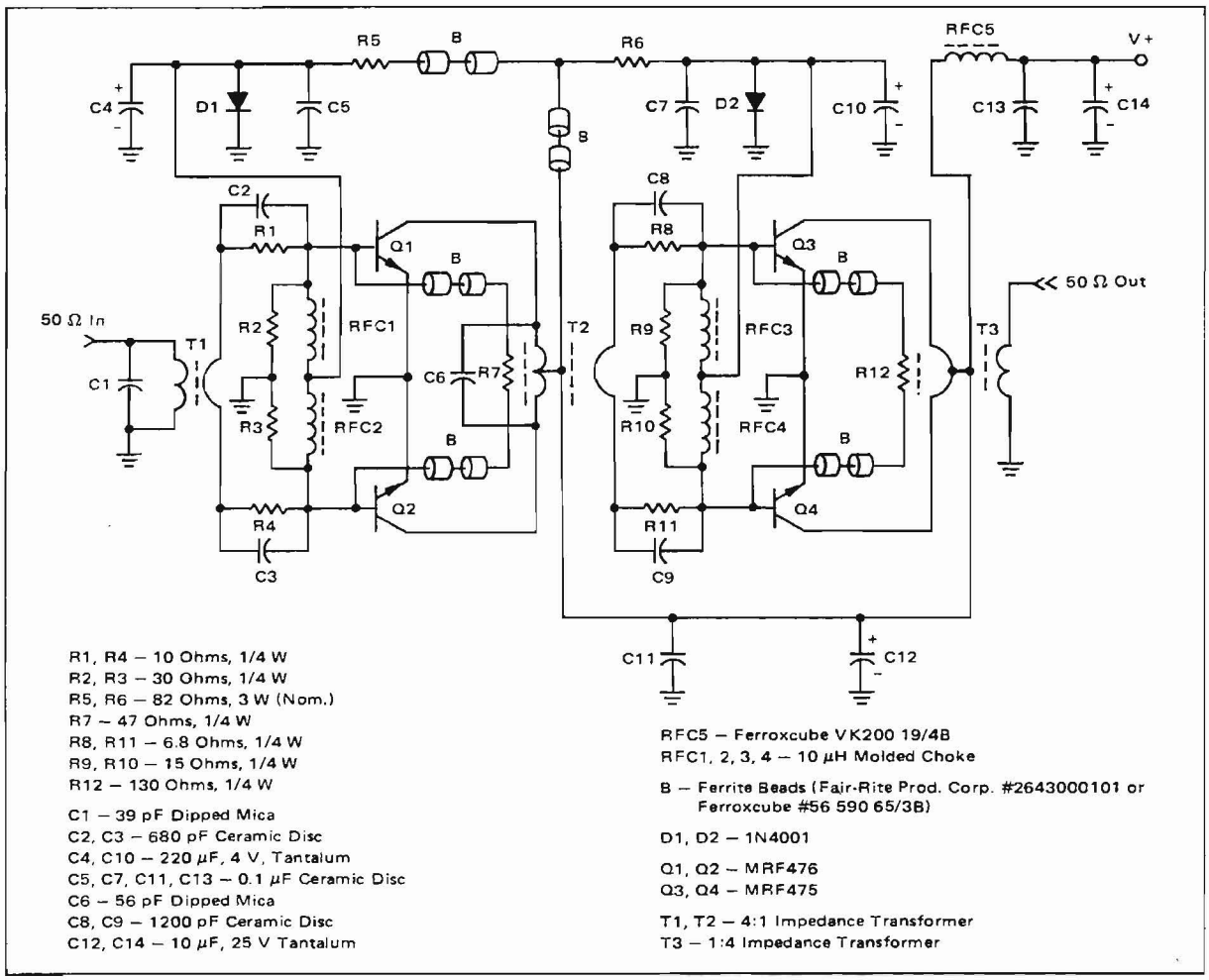

FIGURE 2

The bias currents of each stage are individually adjustable with R5 and R6. Capacitors C4 and C10 function as audio-frequency bypasses to further reduce the source impedance at the frequencies of modulation.

This biasing arrangement is only practical in low and medium power amplifiers, since the minimum current required through the diode must exceed I_C/h_{fe}.

Gain leveling across the band is achieved with simple RC networks in series with the bases, in conjunction with negative feedback. The amplitude of the out-of-phase voltages at the bases is inversely proportional to the frequency as a result of the series inductance in the feedback loop and the increasing input impedance of the transistors at low frequencies. Conversely, the negative feedback lowers the effective input impedance presented to the source (not the input impedance of the device itself) and with proper voltage slope would equalize it. With this technique, it is possible to maintain an input VSWR of 1.5:1 or less from 1.6 to 30 MHz.

Impedance Matching and Transformers

Matching of the input and output impedances to 50 ohms, as well as the interstage matching, is accomplished with broadband transformers (Figures 3 and 4).

Normally only impedance ratios such as 1:1, 4:1, 9:1, etc., are possible with this technique, where the low-impedance winding consists of metal tubes, through which an appropriate number of turns of wire is threaded to form the high-impedance winding. To improve the broadband characteristics, the winding inductance is increased with magnetic material. An advantage of this design is its suitability for large-quantity manufacturing, but it is difficult to find low-loss ferrites with sufficiently high permeabilities for applications where the physical size must be kept small and impedance levels are relatively high. Problems were encountered especially with the output transformer design, where an inductance of 4 µH minimum is required in the one-turn winding across the collectors, when the load impedance is

$$\frac{2(V_{CE} - V_{CEsat})^2}{P_{out}} = \frac{2(13.6 - 2.5)^2}{20} = 12.3 \text{ ohms.}^{4,8}$$

Ferrites having sufficiently low-loss factors at 30 MHz range only up to 800–1000 in permeability and the inductance is limited to 2.5–3.0 µH in the physical size required. This would also limit the operation to approximately 4 MHz, below which excessive harmonics are

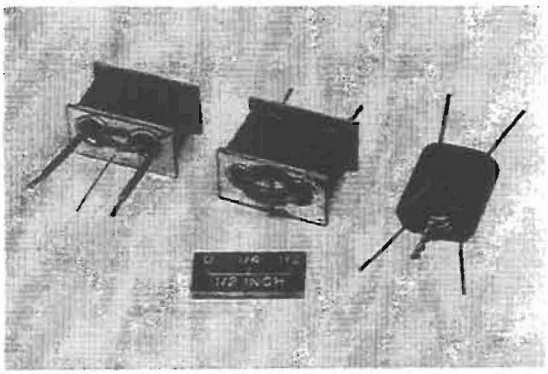

FIGURE 3

Examples of broadband transformers. Variations of these are used in all designs of this article (see text). All ferrites in transformers are Fair-Rite Products Corp. #2643006301 ferrite beads.* The turns ratios shown in Figure 4 are imaginary and do not necessarily lead to correct design practices.

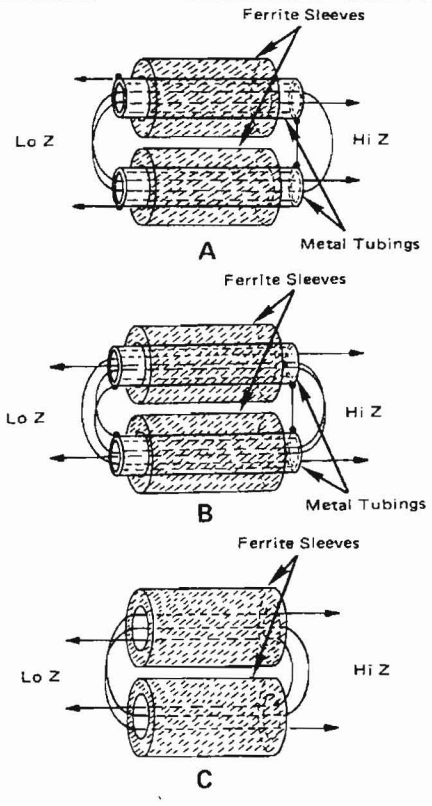

FIGURE 4

generated and the efficiency will degrade. One possible solution is to increase the number of turns, either by using the metal tubes for only part of the windings as in Figure 4B, or simply by winding the two sets of windings randomly through ferrite sleeves or a series of beads (Figures 3C and 4C). In the latter, the metal tubes can be disregarded or can be used only for mounting purposes. T3 was eventually replaced with a transformer of this type, although not shown in Figure 1.

Below approximately 100 MHz, the input impedances of devices of the size of MRF475 and smaller are usually capacitive in reactance, and the X_S is much smaller than the R_S, (Low Q). For practical purposes, we can then use the formula $\sqrt{(R_S^2 + X_S^2)}$ to find the actual input impedance of the device. The data-sheet numbers for 30 MHz are 4.5, -j2.4 ohms, and we get $\sqrt{(4.5^2 + 2.4^2)}$ = 5.1 ohms. The base-to-base impedance in a push-pull circuit would be four times the base-to-emitter impedance of one transistor. However, in Class AB, where the base-emitter junction is forward biased and the conduction angle is increased, the impedance becomes closer to twice that of one device. The rounded number of 11 ohms must then be matched to the driver output. The drive power required with the 10 dB specified minimum gain is

$$P_{out}/Log^{-1}(G_{PE}/10) = 2.0\ W$$

and the driver output impedance using the previous formula is $2(11.1^2)/2$ = 123 ohms. The 11 ohms in series with the gain-leveling networks (C8, R8 and C9, R11) is 17 ohms. The closest practical transformer for this interface would be one with 9:1 impedance ratio. This would present a higher-than-calculated load impedance to the driver collectors, and for the best linearity the output load should be lower than required for the optimum gain and efficiency. Considering that the device input impedance increases at lower frequencies, a better overall match is possible with a 4:1, especially since the negative feedback is limited to only 4 dB at 2 MHz due to its effect on the efficiency and linearity.

The maximum amount of feedback a circuit can tolerate depends much on the physical layout, the parasitic inductances, and impedance levels, since they determine the phase errors in the loop. Thus, in general, the high-level stages should operate with lower feedback than the low-level stages.

The maximum amount of feedback the low-level driver can tolerate without noticeable deterioration in IMD is about 12 dB. This makes the total 16 dB, but from the data sheets we find that the combined gain variation for both devices from 2 to 30 MHz is around 29 dB. The difference, or 13 dB, should be handled by the gain-leveling networks.

The input impedance of the MRF476 is 7.55, -j0.65 ohms at 30 MHz resulting in the base-to-base impedance of 2 x $\sqrt{(7.55^2 + 0.65^2)}$ = 15.2 ohms. This, in series with networks R1, C1 and R4, C3 (2 x 4.4 ohms), gives 24 ohms, and would require a 2:1 impedance ratio transformer for a 50-ohm interface. However, due to the influence of strong negative feedback in this stage, a better overall matching is possible with 4:1 ratio. The input networks were designed in a manner similar to that described in Reference 8.

*Wallkill, N.Y. 12589

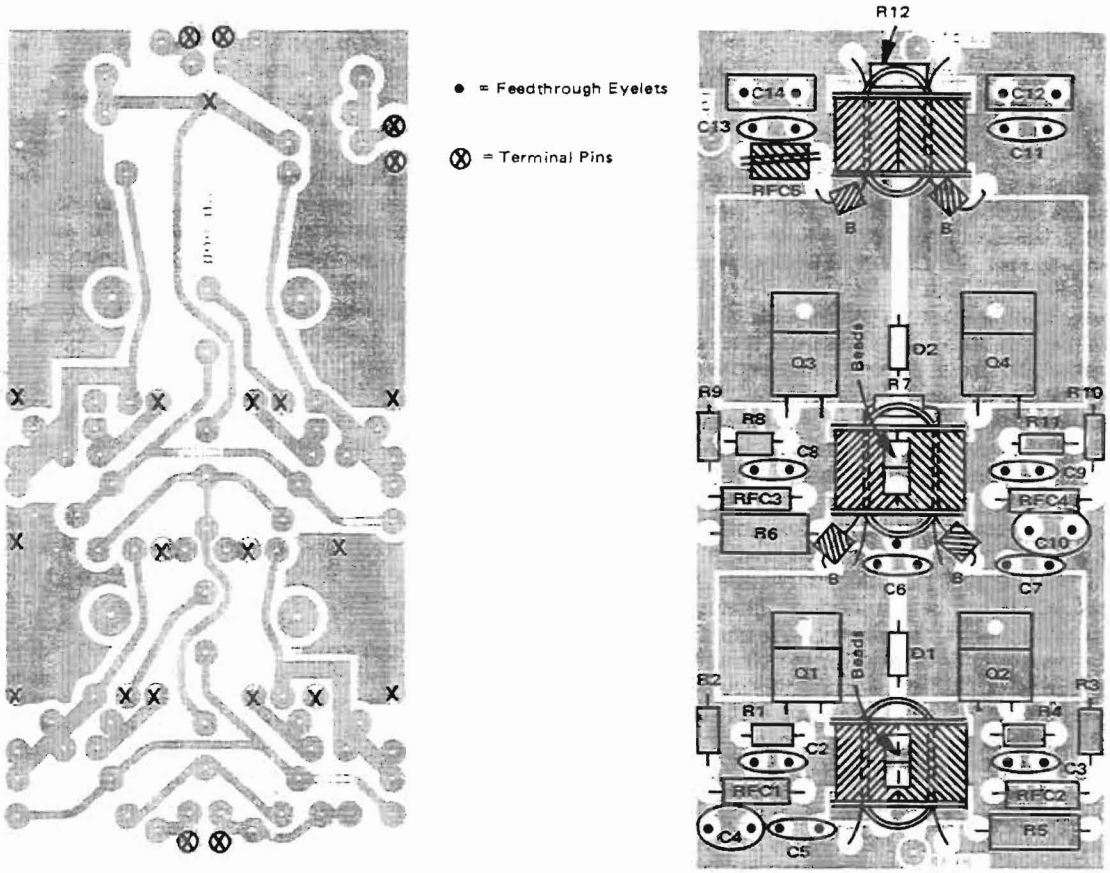

FIGURE 5
Component Layout Diagram of Low-Cost 20 W Amplifier

The leads of R7 and R12 form the one-turn feedback windings in T2 and T3. Ferrite beads in dc line can be seen located under T1 and T2.

Measurements and Performance Data

At a power output of 20 W CW, all output harmonics were measured about 30 dB or more below the fundamental, except for the third harmonic which was only attenuated 17 dB to 18 dB at frequencies below 5 MHz. Typical numbers for the higher order distortion products (d_9 and d_{11}) are in the order of -60 dB above 7 MHz and -50 dB to -55 dB at the lower frequencies. These both can be substantially reduced by increasing the idle currents, but larger heat sinks would be necessary to accommodate the increased dissipation.

The efficiency shown in Figure 6 represents the overall figure for both stages. Currents through the bias networks, which are 82/(13.6 - 0.7) = 0.16 A each, are excluded. Modified values for R5 and R6 may have to be selected, depending on the forward voltage characteristics of D1 and D2.

Although this amplifier was designed to serve as a 1.6 to 30 MHz broadband driver, it is suitable for the citizens band use as well. With some modifications and design shortcuts, the optimization can be concentrated to one frequency.

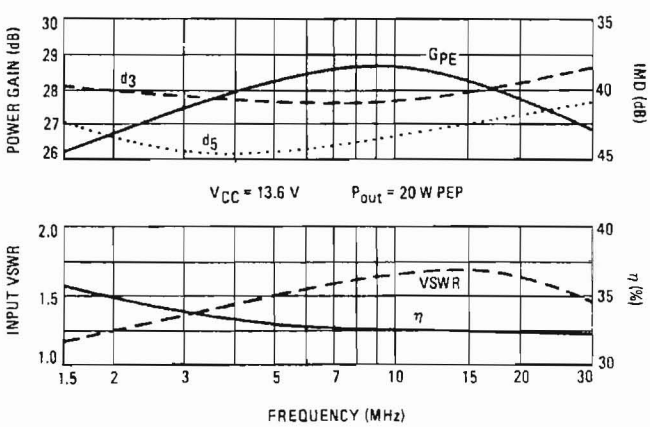

FIGURE 6

Intermodulation distortion and power gain versus frequency (upper curves).

Input VSWR and combined collector efficiency of both stages (lower curves).

20 W, 55 dB HIGH PERFORMANCE DRIVER
12-Volt Version

The second amplifier employs the MHW591 hybrid module to drive a pair of larger devices which can be operated Class A or AB, depending on the requirements. Transistors such as MRF449 and MRF455 are recommended for Class A and MRF433 for Class AB operation. A 24–28 volt version with MHW592 and a pair of MRF401s was also designed, and some of the test data will be presented. For Class A, the power parts should be replaced with MRF426s.*

These amplifiers are a good example of how a good gain flatness can be achieved across the four-octave band, with simple RC input networks and negative feedback, while maintaining a reasonable input VSWR.

The MHW591 is employed as a predriver in this unit. The MHW591 and its counterpart, MHW592, were developed for low-level SSB driver applications from 1.0 MHz to 250 MHz. The Class A operation results in a steady-state current drain of approximately 0.32 A, which does not vary with the signal level. At an output level of 600 mW PEP, the IMD is typically better than -40 dB, which can be considered sufficiently good for most purposes. Since the power gain is specified as 36.5 dB, the maximum drive level for the 600 mW output is 0.13 mW, or -9 dBM. For the final power output of 20 W, a power gain of 15.2 dB minimum is required at the highest operating frequency for the power transistors. A good, inexpensive device for this is the MRF433, which has a 20 dB minimum gain and -30 dB IMD specification at an output level of 12.5 W PEP. The push-pull configuration, due to inconsistent ground planes and broadbanding due to matching compromises usually results in 2 dB to 3 dB gain losses from figures measured in a test fixture. Assuming a transistor power gain of 18 dB, the total will be 54.5 dB, representing an input power of -11 dBM. Later measurements, however, indicated a gain of 56 dB (±0.5 dB) at the specified power output, making the input level around -13 dBM.

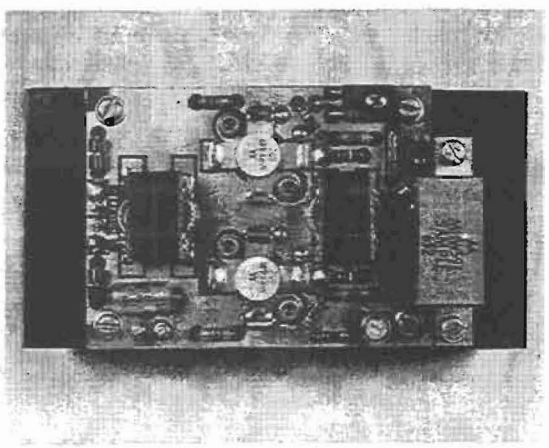

FIGURE 7

Biasing and Feedback

The bias circuit employed with this amplifier is basically similar to the one described earlier, with the exception of having an emitter follower output. A second diode in series with the one normally seen with the clamping diode method compensates for the voltage drop in the base-emitter junction of the emitter follower, Q1 (Figure 8). The minimum current through D1 and D2 is (I_C/h_{FE}) (Q2 + Q3)/h_{FE}(Q1), and in this case (2.5/40)/40 = 1.5 mA. Typical h_{FE} for the MRF433 is 40, and with the devices biased to 200 mA each, the standby base current is 10 mA. In operation the load current of Q1 then varies between 10 and 62 mA. A Case 77 transistor exhibiting low variations in base-emitter saturation voltage over this current range is MJE240. Base-emitter saturation voltage determines the bias source impedance, which should not exceed approximately 0.3 ohm, representing a 20 mV variation in voltage from idle to full drive conditions. If source impedance exceeds 0.3 ohms, a capacitor of 500–1000 μF should be connected from the emitter of Q1 to ground.

The peak dissipation of Q2 is under one watt, making it possible to mount the transistor directly to the circuit board without requiring any additional heat sinking.

Diodes D1 and D2 are located on the lower side of the board, near Q2 and Q3 (Figure 9). The leads are formed to allow the diodes to come into contact with the transistor flanges. The thermal contact achieved in this manner is not the best possible, even when the gaps are filled with silicone compound, but the thermal time constant is lower than with most other methods. Both diodes are used for temperature tracking, although the voltage drop of only one is required to compensate for the V_{BE} forward drop of Q1. The advantages of this circuit are simplicity, low standby current drain, and ease of adjustment with a small trimpot.

The voltages for the negative feedback are derived separately from the collectors of Q2 and Q3 through L6, R6 and L7, R7. Capacitors C5 and C6 are used for dc isolation. Because of the high RF voltage levels on the collectors, this method is only feasible in low- and medium-power amplifiers. At higher power levels, the power-handling requirements for the series resistors (Figure 8), which must be noninductive, become impractical. A feedback voltage source with lower impedance must be provided in such cases.[8]

The MRF433 has a higher figure of merit (emitter periphery/base area) than the MRF475, for example. This results in smaller differences in power gain per given bandwidth, since the device is operating farther away from the 6 dB/octave slope.[9] Disregarding the package inductances, which affect the Q, the higher figure of merit makes such devices more suitable for broadband operation. The 2 MHz to 30 MHz ΔG_{PE} of the MRF433 is 8 dB, which is divided equally between the negative feedback and the leveling networks C3, R4 and C4, R5. The 2 MHz and 30 MHz impedance values are 9.1, -j3.5 and 2.5, -j2.2 ohms, respectively, although the 2 MHz values are not given in the data sheet.

At 30 MHz we can first determine what type of transformer is needed for the 50-ohm input interface. The effective transformer load impedance is $2\sqrt{(2.5^2 + 2.2^2)}$ + 2(2.4) ohms (leveling networks) = 11.5 ohms, which indicates that a 4:1 impedance ratio is the closest possible (see Figures 3B, 4A, and 8). These values are accurate for practical purposes, but they are not exact, since part of the capacitive reactance in C3 and C4 will be cancelled, depending on the transformer characteristics.

*To be introduced.

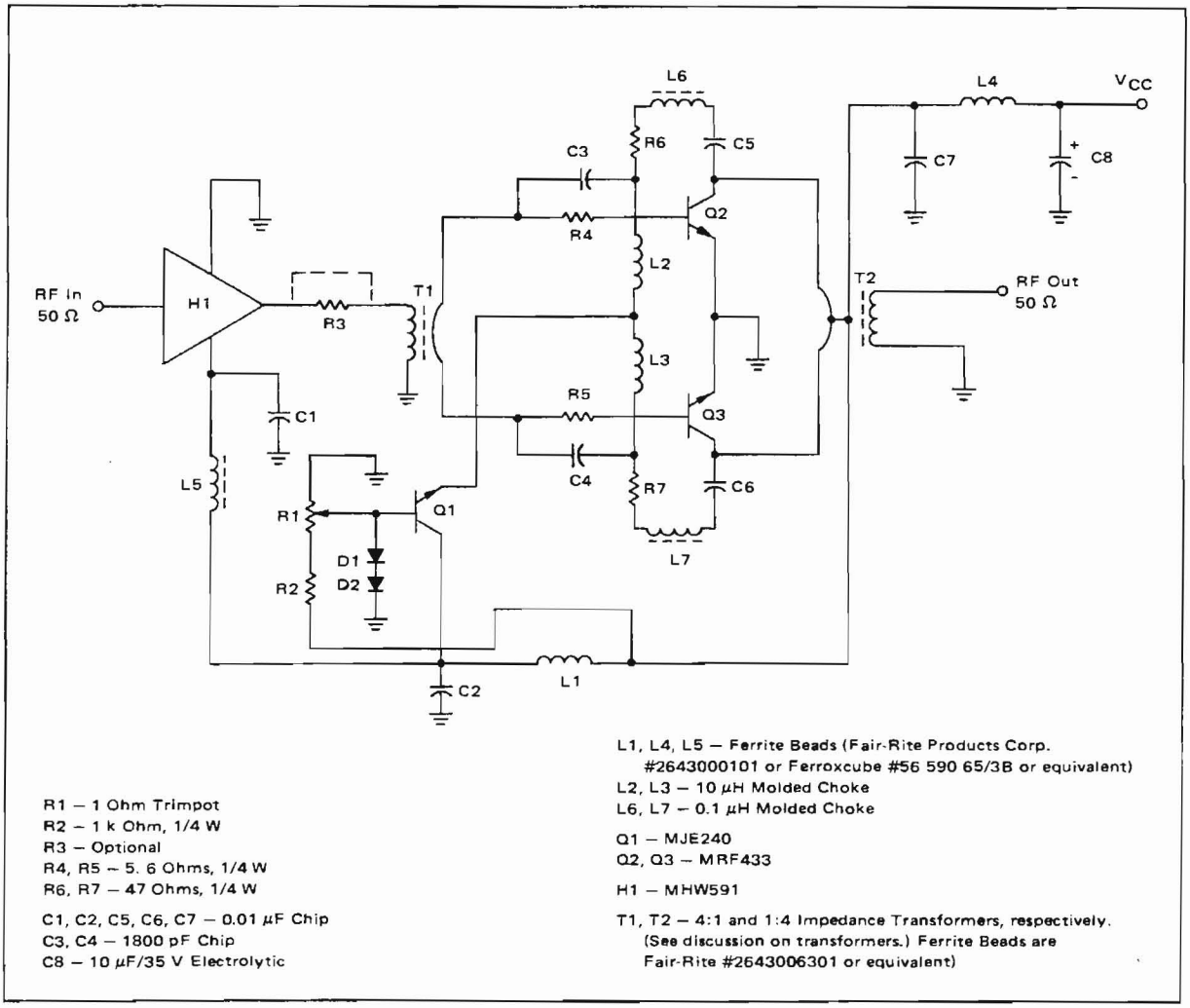

FIGURE 8

The output matching is done with a transformer similar to that described in the first part of this paper (Figures 4B, 4C). This transformer employs a multi-turn primary, which can be provided with a center tap for the collector dc feed. In addition to a higher primary inductance, more effective coupling between the two transformer halves is obtained, which is important regarding the even-order harmonic suppression.

28-Volt Version

A 28-V version of this unit has also been designed with the MHW592 and a pair of MRF401s. The only major change required is the output transformer, which should have a 1:1 impedance ratio in this case. The transformer consists of six turns of RG-196 coaxial cable wound on an Indiana General F-627-8-Q1 toroid. Each end of the braid is connected to the collectors, and the inner conductor forms the secondary. A connection is made in the center of the braid (three turns from each end) to form the center tap and dc feed.

The MRF433 and MRF401 have almost similar input characteristics, and no changes are necessary in the input circuit, except for the series feedback resistors, which should be 68–82 ohms and 1 W.

In designing the gain-leveling networks, another approach can be taken, which does not involve the computer program described in Reference 8. Although the input VSWR is not optimized, it has proved to give satisfactory results.

The amount of negative feedback is difficult to determine, as it depends on the device type and size and the physical circuit layout. The operating voltage has a minimal effect on the transistor input characteristics, which are more determined by the electrical size of the die. High-power transistors have lower input impedances and higher capacitances, and phase errors are more likely to occur due to circuit inductances.

Since the input capacitance is an indication of electrical size of the device, we can take the paralleled value (X_p) at 2 MHz, which is $X_S + (R_S^2/X_S)$ and for MRF433 $3.5 + (9.1^2/3.5) = 27$ ohms. The X_p of the largest devices available today is around 10 ohms at 30 MHz, and experience has shown that the maximum feedback should be limited to about 5 dB in such case. Using these figures

as constants, and assuming the G_{PE} is at least 10 dB, we can estimate the amount of feedback as: $5/(10^2/27) + 5 = 6.35$ dB, although only 4 dB was necessary in this design due to the low ΔG_{PE} of the devices.

The series base resistors (R4 and R5) can be calculated for 4 dB loss as follows:

$$\frac{[(V_{in} \times \Delta 4dB) - V_{in}]}{I_{in}} = \frac{[(0.79 \times 1.58) - 0.79]}{0.04}$$

$$= 11.45 \text{ ohms, or}$$

$$11.45/2 = 5.72 \text{ ohms each.}$$

$Z_{in}(2\text{ MHz}) = \sqrt{(9.1^2 + 3.5^2)} = 9.75$ ohms, in Class AB push-pull 19.5 ohms.

$P_{in} = 20\text{ W} - 28\text{ dB} = 20/630 = 0.032\text{ W}$

V_{RMS} (base to base) $= \sqrt{(0.032 \times 19.5)} = 0.79\text{ V}$

$I_{in} = V_{in}/R_{in} = 0.79/19.5 = 0.04\text{ A}$

$\Delta V4\text{ dB} = \sqrt{[\text{Log}^{-1}(4/10)]} = 1.58\text{ V}$

The parallel capacitors (C3 and C4) should be selected to resonate with R (5.7 ohms) somewhere in the mid-band. At 15 MHz, out of the standard values, 1800 pF appears to be the closest, having a negligible reactance at 2 MHz, and 2.8 ohms at 30 MHz, where most of the capacitive reactance is cancelled by the transformer winding inductance.

Measurements and Performance Data

The output harmonic contents of this amplifier are substantially lower than normally seen in a Class AB system operating at this power level and having a 4.5-octave bandwidth. All harmonics except the third are attenuated more than 30 dB across the band. Between 20 and 30 MHz, -40 to -55 dB is typical. The third harmonic

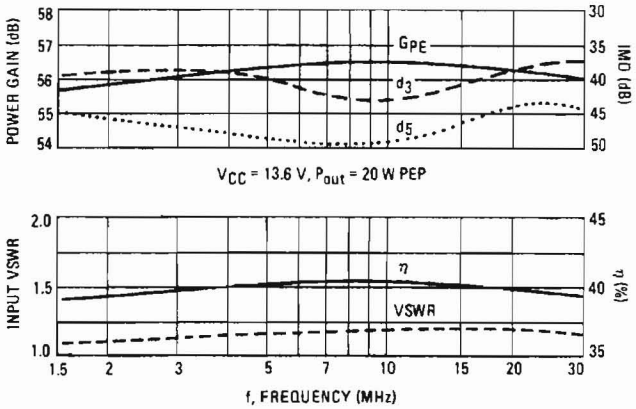

FIGURE 10

Intermodulation Distortion and Power Gain versus Frequency (Upper Curves). Input VSWR and Collector Efficiency (excluding MHW591) (Lower Curves).

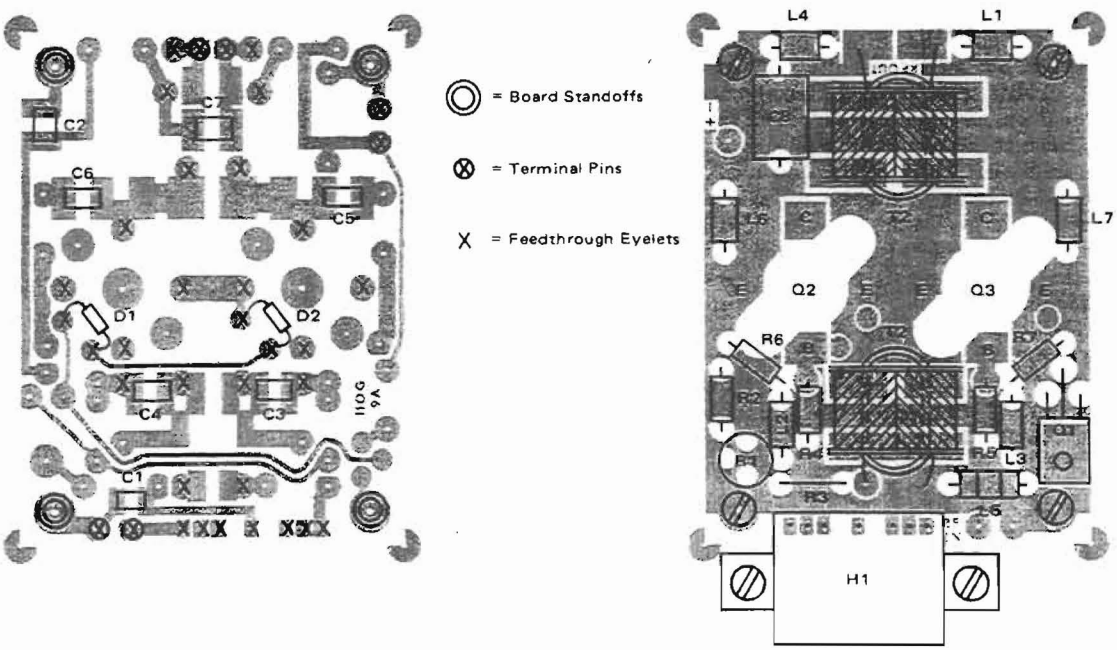

FIGURE 9
Component Layout Diagram of
20 W, 55 dB High-Performance Driver

The leads of D1 and D2 are bent to allow the diodes to contact the transistor mounting flanges.

Note that the mounting pad of Q1 must be connected to the lower side of the board through an eyelet or a plated through-hole.

has its highest amplitude (-20 to -22 dB), as can be expected, below 20 MHz. The measurements were done at an output level of 20 W CW and with 200 mA collector idle current per device. Increasing it to 400 mA improves these numbers by 3–4 dB, and also reduces the amplitudes of d_5, d_7, d_9, and d_{11} by an average of 10 dB, but at the cost of 2–3 dB higher d_3.

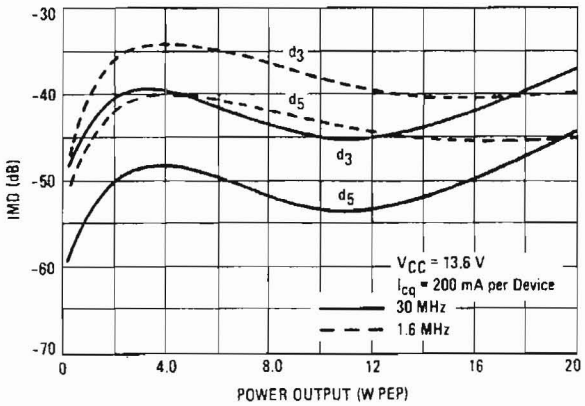

FIGURE 11 – IMD versus Power Output

CONCLUSION

The stability of both designs (excluding the 28 V unit) was tested into reactive loads using a setup described in Reference 8. Both were found to be stable into 5:1 load mismatch up to 7 MHz, 10:1 up to 30 MHz, except the latter design did not exhibit breakups even at 30:1 in the 20–30 MHz range. If the test is performed under two-tone conditions, where the power output varies from zero to maximum at the rate of the frequency difference, it is easy to see at once if instabilities occur at any power level.

The two-tone source employed in all tests consists of a pair of crystal oscillators, separated by 1 kHz, at each test frequency. The IMD (d_3) is typically -60 dB and the harmonics -70 dB when one oscillator is disconnected for CW measurements.

HP435 power meters were used with Anzac CH-130-4 and CD-920-4 directional couplers and appropriate attenuators. Other instruments included HP141T analyzer system and Tektronix 7704A oscilloscope-spectrum analyzer combination.

REFERENCES

1. "Linearized Class B Transistor Amplifiers," IEEE Journal of Solid State Circuits, Vol. SC-11, No. 2, April, 1976.

2. Pappenfus, Bruene and Schoenike, "Single Sideband Principles and Circuits," McGraw-Hill.

3. Reference Data for Radio Engineers, ITT, Howard & Sams Co., Inc.

4. H. Grandberg, "Broadband Transformers and Power Combining Techniques for RF," AN-749, Motorola Semiconductor Products Inc.

5. H. Grandberg, "Measuring the Intermodulation Distortion of Linear Amplifiers," EB-38, Motorola Semiconductor Products Inc.

6. K. Simons, Technical Handbook for CATV Systems, Third Edition, Jerrold Electronics Corp.

7. Data Sheets, Motorola MRF475, MRF476, MRF433, and MHW591

8. H. Grandberg, "Two-Stage 1 KW Solid-State Linear Amplifier," AN-758, Motorola Semiconductor Products Inc.

9. Phillips, "Transistor Engineering," McGraw-Hill.

Literature Distribution Centers:
USA: Motorola Literature Distribution; P.O. Box 20912; Phoenix, Arizona 85036.
EUROPE: Motorola Ltd.; European Literature Centre; 88 Tanners Drive, Blakelands, Milton Keynes, MK14 5BP, England.
JAPAN: Nippon Motorola Ltd.; 4-32-1, Nishi-Gotanda, Shinagawa-ku, Tokyo 141, Japan.
ASIA PACIFIC: Motorola Semiconductors H.K. Ltd.; Silicon Harbour Center, No. 2 Dai King Street, Tai Po Industrial Estate, Tai Po, N.T., Hong Kong.

MOTOROLA

11188-4 PRINTED IN USA (1994) MPS/POD YBACAA

AN779/D

EB-27A

COMMUNICATIONS

Engineering Bulletin

By: Helge Granberg
Circuits Engineer, SSB

Get 300 Watts PEP Linear Across 2 To 30 MHz From This Push-Pull Amplifier

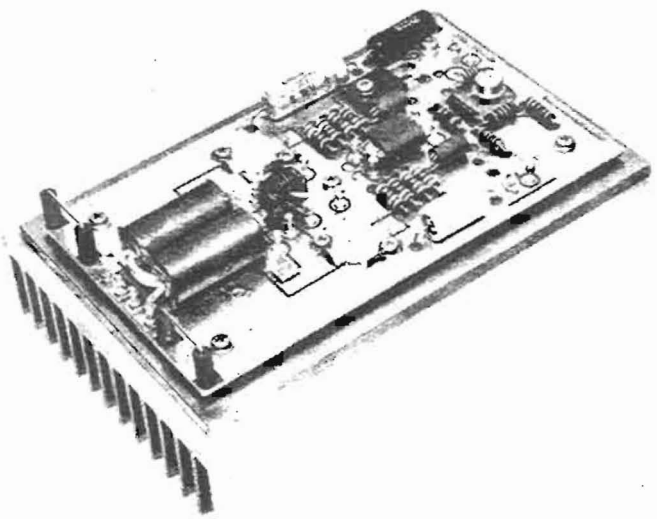

(The heat sink shown with amplifier is sufficient only for short test periods under forced air cooling.)

This bulletin supplies sufficient information to build a push-pull linear amplifier for 300 watts of PEP or CW output power across the 2- to 30-MHz band. One of Motorola's new high-power transistors developed for single-sideband, MRF422, is used in this application.

Like all transistors in its family of devices, MRF422 combines single-chip construction that is advancing the state-of-the-art, and improved packaging to accommodate the low collector efficiencies encountered in class B operation. Rated maximum output power is 150 watts CW or PEP with intermodulation distortion spec'd at −30 dB maximum, −33 dB typical. Although not recommended, a saturated power level of 240- to 250-W is achievable. Maximum allowable dissipation is 300 W at 25°C.

Because of its excellent load and line voltage regulating capabilities, an integrated circuit bias regulator is used in the amplifier. The MPC1000, originally described in this bulletin, consisted of a MC1723 chip and a built-in pass transistor. The manufacture of this device has been discontinued however, and the board lay-out was modified to incorporate the above two in separate packages. The load regulation typically measures less than 2% at current levels up to 0.5 A, which assumes an h_{FE} of 40 for the RF power devices. The board surface provides a sufficient heat sink for the 2N5990 pass transistor, but a separate heat dissipator, such as Thermalloy 6107 can be added if necessary. With the component values shown, the bias is adjustable from 0.4 to 0.8 volts.

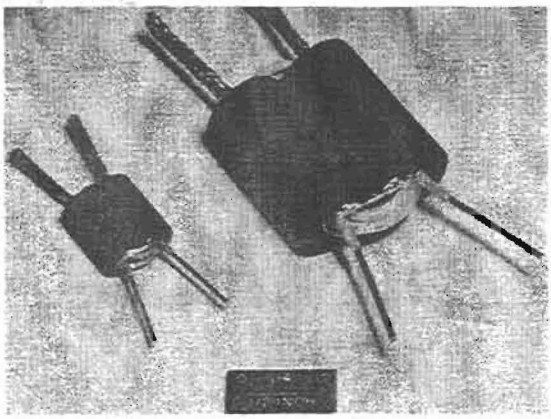

Transformer Construction

Gain flatness over the band is achieved using base input networks R_1C_2 and R_2C_3 and negative feedback through R_3 and R_4. The networks represent a series reactance of 0.69 ohms at 30 MHz rising to 1.48 ohms at 2 MHz. A single-turn winding in the collector choke provides a low-impedance negative feedback source, thus R_3 and R_4 determine the amount. The reactance of C_4 reduces feedback at high frequencies with the result that feedback increases an average of 4 dB per octave at decreasing frequency.

For continuous operation at full power CW, it is recommended that heat sink compound, such as Dow Corning #340, be applied between the board surface and R_3 and R_4, and if possible have air circulating over the top of the circuit board as well.

The effective base-to-base impedance, increased by the RC networks is about 5 ohms at midband. As a result of this and the 9:1 impedance ratio in the input transformer T1, the input VSWR is limited to 1.9:1 or less across the band. Transformer T2, in addition to providing a source for the feedback and carrying the dc collector current, acts as the rf center tap of the output transformer. To construct T2, wind 5 turns of 2 twisted pairs of AWG No. 22 enameled wire on a Stackpole 57-9322 toroid (Indiana General F627-8Q1).

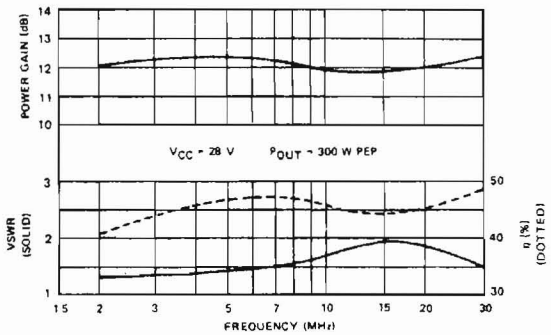

Figure 1 — Collector Efficiency, Power Gain and VSWR vs Frequency

A Stackpole dual balun ferrite core 57-1845-24B is used for T1. The secondary is made of ⅛" copper braid, through which three turns of the primary winding (No. 22 Teflon® insulated hook-up wire) are threaded. The construction of T3 is similar to that of T1. It employs two Stackpole 57-3238* ferrite sleeves which are cemented together for easier construction. The primary is made of ¼" copper braid, through which three turns of No. 16 Teflon® insulated wire are threaded for the secondary.

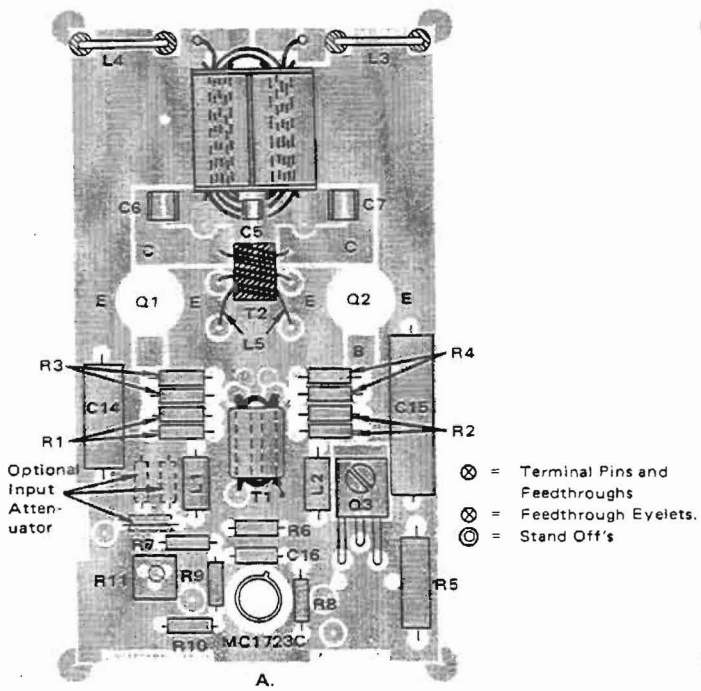

A.

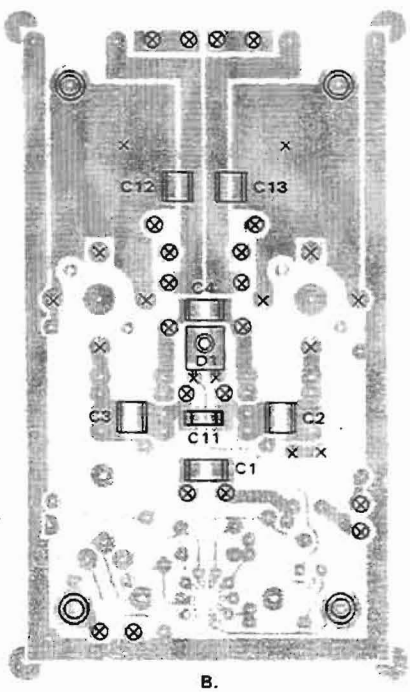

B.

300-Watt Linear Amplifier Schematic Diagram

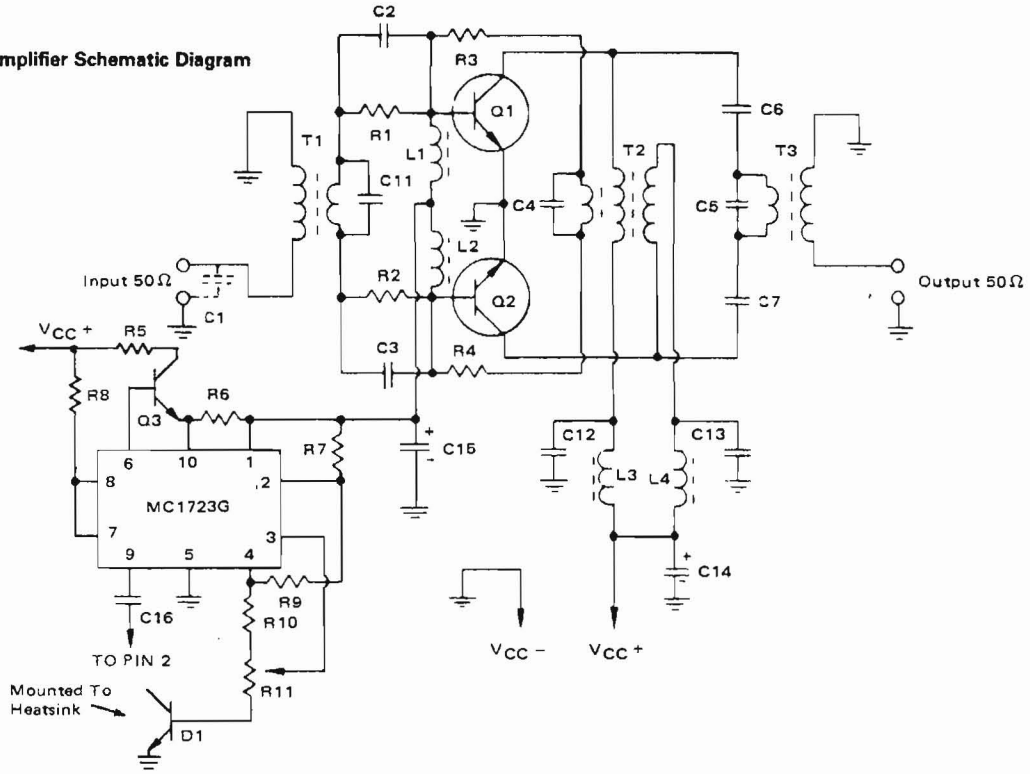

C1 – 100 pF
C2, C3 – 5600 pF
C4, C5 – 680 pF
C6, C7 – 0.10 μF
C11 – 470 pF
C12, C13 – 0.33 μF
C14 – 10 μF – 50 V electrolytic
C15 – 500 μF – 3 V electrolytic
C16 – 1000 pF

R1, R2 – 2 X 3.3Ω, 1/2 W in parallel
R3, R4 – 2 X 3.9Ω, 1/2 W in parallel
R5 – 47Ω, 5 W
R6 – 1.0Ω, 1/2 W
R7, R8 – 1.0 k, 1/2 W
R9 – 18 k, 1/2 W
R10 – 8.2 k, 1/2 W
R11 – 1.0 k Trimpot
D1 – 2N5190
L1, L2 – Ferroxcube VK200 20/48
L3, L4 – 6 ferrite beads each, Ferroxcube 56590 65/38

Q1, Q2 – MRF422, Q3 – 2N5990
T1, T2, T3 – See text

All capacitors except electrolytics and C16 are chips –

Union Carbide type 1813 and 1225, or Varadyne size 18 or 14, or equivalent

For production quantities, the braid in T_3 may be made of brass or copper tubes with their ends soldered to pieces of PC board laminate. See cover picture and Motorola AN-749 for details.

The bandwidth characteristics of these transformers do not equal those of the transmission line type, but they're much easier to duplicate.

The measured performance of the amplifier is shown in figures 1, 2, and 3 and harmonic rejection data in table I.

Table I. Output harmonic contents, measured at 300-W CW (all test data taken using a tuned output, narrow band signal source).

	2nd	3rd	4th	5th
f (Mhz)	(dB below the carrier)			
30.0	−38	−25	−34	−48
20.0	−33	−13	−43	−45
15.0	−50	−10	−51	−47
7.50	−40	−30	−55	−47
4.0	−37	−22	−55	−37
2.0	−36	−18	−45	−37

*A similar product is available from Fair-Rite Products Corp., Wallkill, N.Y., 12589

®Registered trademark of DuPont

PCB, chips capacitors, transformers T_1, T_2, T_3, and ferrite beads are available from: COMMUNICATIONS CONCEPTS, 2648 N. Aragon Ave., Kettering, Ohio 45420. Telephone: (513) 294-8425.

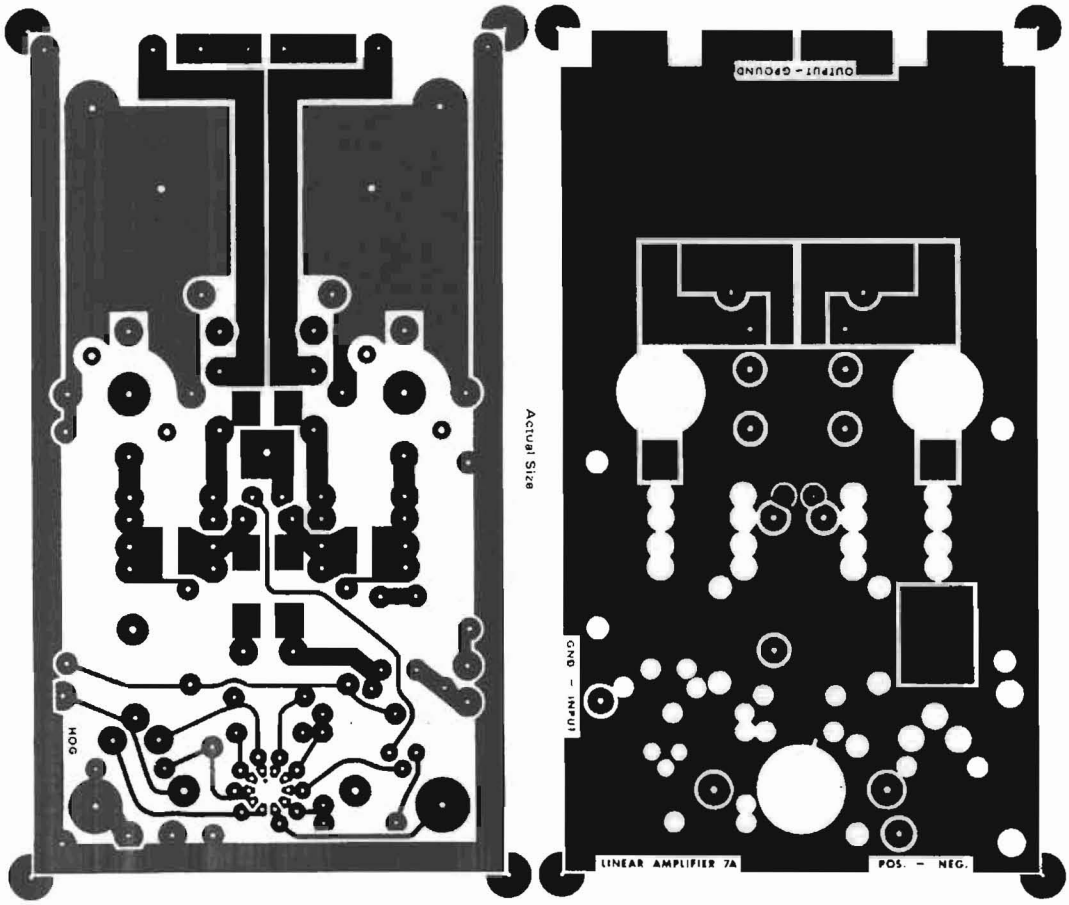

Figure 2 — IMD vs Frequency

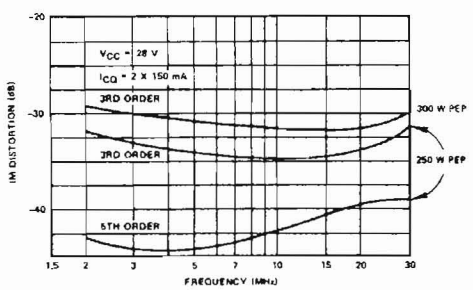

Figure 3 — IMD vs Power Output

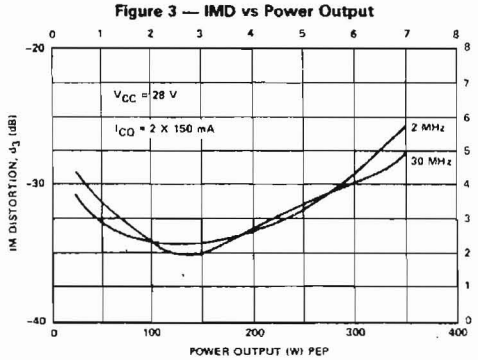

Literature Distribution Centers:
USA: Motorola Literature Distribution; P.O. Box 20912; Phoenix, Arizona 85036.
EUROPE: Motorola Ltd.; European Literature Centre; 88 Tanners Drive, Blakelands, Milton Keynes, MK14 5BP, England.
JAPAN: Nippon Motorola Ltd.; 4-32-1, Nishi-Gotanda, Shinagawa-ku, Tokyo 141, Japan.
ASIA PACIFIC: Motorola Semiconductors H.K. Ltd.; Silicon Harbour Center, No. 2 Dai King Street, Tai Po Industrial Estate, Tai Po, N.T., Hong Kong.

MOTOROLA

24887-1 PRINTED IN USA (9/93) MPS/POD

EB27A/D